Journal of Hydrology 633 (2024) 130968

Contents lists available at ScienceDirect

Journal of Hydrology

journal homepage: www.elsevier.com/locate/jhydrol

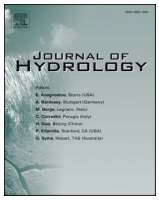

Research papers

Utilizing machine learning and CMIP6 projections for short-term agricultural drought monitoring in central Europe (1900–2100)

Safwan Mohammed [a,b,*], Sana Arshad [c], Firas Alsilibe [d], Muhammad Farhan Ul Moazzam [e,i], Bashar Bashir [f], Foyez Ahmed Prodhan [g,h], Abdullah Alsalman [f], Attila Vad [a], Tamás Ratonyi [a], Endre Harsányi [a,b]

[a] Institute of Land Use, Technical and Precision Technology, Faculty of Agricultural and Food Sciences and Environmental Management, University of Debrecen, Debrecen 4032, Hungary
[b] Institutes for Agricultural Research and Educational Farm, University of Debrecen, Böszörményi 138, 4032 Debrecen, Hungary
[c] Department of Geography, The Islamia University of Bahawalpur, Bahawalpur 63100, Pakistan
[d] Department of Transport Infrastructure and Water Resources Engineering, Széchenyi István University, Egyetem tér 1, 9026 Gyor, Hungary
[e] Department of Civil Engineering, College of Ocean Science, Jeju National University, 102 jejudaehakro, Jeju 63243, Republic of Korea
[f] Department of Civil Engineering, College of Engineering, King Saud University, P.O. Box 800, Riyadh 11421, Saudi Arabia
[g] Weather and Climate Modeling Laboratory, Institute of Climate Change and Environment, Bangabandhu Sheikh Mujibur Rahman Agricultural University, Gazipur 1706, Bangladesh
[h] Department of Agricultural Extension and Rural Development, Bangabandhu Sheikh Mujibur Rahman Agricultural University, Gazipur 1706, Bangladesh
[i] Department of Civil and Environmental Engineering, Pusan National University, Busan 46241, Republic of Korea

ARTICLE INFO

This manuscript was handled by Emmanouil Anagnostou, Editor-in-Chief

Keywords:
Standardized precipitation index
Forecasting
CMIP6
Random Forest
Hungary

ABSTRACT

Water availability for agricultural practices is dynamically influenced by climatic variables, particularly droughts. Consequently, the assessment of drought events is directly related to the strategic water management in the agricultural sector. The application of machine learning (ML) algorithms in different scenarios of climatic variables is a new approach that needs to be evaluated. In this context, the current research aims to forecast short-term drought i.e., SPI-3 from different climatic predictors under historical (1901–2020) and future (2021–2100) climatic scenarios employing machine learning (bagging (BG), random forest (RF), decision table (DT), and M5P) algorithms in Hungary, Central Europe. Three meteorological stations namely, Budapest (BD) (central Hungary), Szeged (SZ) (east south Hungary), and Szombathely (SzO) (west Hungary) were selected to forecast short-term agriculture drought i.e., Standardized Precipitation Index (SPI-3) in the long run. For this purpose, the ensemble means of three global circulation models GCMs from CMIP6 are being used to get the projected (2021–2100) time series of climatic indicators (i.e., rainfall R, mean temperature T, maximum temperature T_{max}, and minimum temperature T_{min} under two scenarios of socioeconomic pathways (SSP2-4.5 and SSP4-6.0). The results of this study revealed more severe to extreme drought events in past decades, which are projected to increase in the near future (2021–2040). Man-Kendall test (Tau) along with Sen's slope (SS) also revealed an increasing trend of SPI-3 drought in the historical period with Tau = −0.2, SS = −0.05, and near future with Tau = −0.12, SS = −0.09 in SSP2-4.5 and Tau = −0.1, SS = −0.08 in SSP4-6.0. Implementation of ML algorithms in three scenarios: SC1 ($R + T + T_{max} + T_{min}$), SC2 ($R$), and SC3 ($R + T$)) at the BD station revealed RF-SC3 with the lowest RMSE $_{RFSC3\text{-}TR} = 0.33$, and the highest NSE $_{RFSC3\text{-}TR} = 0.89$ performed best for forecasting SPI-3 on historical dataset. Hence, the best selected RF-SC3 was implemented on the remaining two stations (SZ and SzO) to forecast SPI-3 from 1901 to 2100 under SSP2-4.5 and SSP4-6.0. Interestingly, RF-SC3 forecasted the SPI-3 under SSP2-4.5, with the lowest RMSE = 0.34 and NSE = 0.88 at SZ and RMSE = 0.34 and NSE = 0.87 at SzO station for SSP2-4.5. Hence, our research findings recommend using SSP2-4.5, to provide more accurate drought predictions from $R + T$ for future projections. This could foster a gradual shift towards sustainability and improve water management resources. However, concrete strategic plans are still needed to mitigate the negative impacts of the projected extreme drought events in 2028, 2030, 2031, and 2034. Finally, the validation of RF for

* Corresponding author at: Institutes for Agricultural Research and Educational Farm, University of Debrecen, Böszörményi 138, 4032 Debrecen, Hungary.
E-mail address: safwan@agr.unideb.hu (S. Mohammed).

https://doi.org/10.1016/j.jhydrol.2024.130968

Available online 28 February 2024

short-term drought prediction on a large historical dataset makes it significant for use in other drought studies and facilitates decision making for future disaster management strategies.

1. Introduction

Drought is a chronic and frequent global natural disaster attributed to climatic change (Spinoni et al., 2019). The intricate and prolonged interplay of hydrological and atmospheric processes, intensified by human activities, causes uncertainties in atmospheric phenomenon, such as precipitation. This influences water balance and intensifies the occurrence of extreme events. (Qiu et al., 2023; Xu et al., 2023). The Intergovernmental Panel on Climate Change (IPCC) sixth assessment report (AR6) reported that climatic-induced extreme events, such as drought, heatwaves, wildfires, heavy rains, and floods, are at high risk in the future at a warming level of 1.0–1.5 °C, with devastating impacts (Alsafadi et al., 2023; Magnan et al., 2021; Pörtner et al., 2022). Drought is one of the most recurring extreme events that is influenced by prolonged and abnormal deficiency of precipitation over a specific region and time, with multifaceted direct or indirect effects on the hydrological subsystem, agriculture, and economy (Arshad et al., 2023b; Blauhut et al., 2022). Droughts are multiscale and multidimensional events characterized by frequency (*f*), duration (*d*), and severity (*S*) at different timescales of short-term (one-month to three-month), medium-term (six-month to twelve-month), and long-term up to thirty-six- months (Wu et al., 2021). Short-term meteorological droughts of 1 to 3 months mostly reflect the deficit of soil moisture conditions, which, if continued to medium to long-term, cause agricultural droughts that restrict crop growth, leading to yield loss (Li et al., 2020; Zhao et al., 2023).

Although drought is a global phenomenon, Europe is often referred to as a 'hotspot' for drought occurrences. In the last decade, a gradual increase in air temperature along with extreme heat waves and high evapotranspiration has accelerated the frequency of drought events in southern and central European regions (Cook et al., 2020; Hari et al., 2020a; Ionita and Nagavciuc, 2021). Regional climatic simulations have revealed that the central and northern European regions are considerably affected by water imbalances due to intensive temperature and changes in precipitation patterns, resulting in persistent and frequent drought events (Nikulin et al., 2011). European summer droughts of 2003 and 2015, with exceptionally high temperatures, increased the vulnerability of the region towards compound extreme events (Hänsel et al., 2019; Ionita et al., 2017; Luterbacher et al., 2004; Schär et al., 2004). It was followed by another extreme drought year in 2018 at 3 °C above long-term mean temperature and devastating impacts in central and northeastern Europe (Hari et al., 2020a; Oikonomou et al., 2020; Schuldt et al., 2020). Therefore, in the last two decades, the drought hazard has become one of the greatest concerns for the European region and is expected to rise more in the 21st century (Buzási et al., 2021). In this context, future drought events were predicted to be more prevalent in Europe (Adeyeri et al., 2023; Iranshahi et al., 2023; Othman and Tukimat, 2023; Samantaray et al., 2022; Wang et al., 2021).

The Standardized Precipitation Index (SPI) introduced by McKee et al. (1993) is a widely adopted precipitation-based drought index that provides a true representation of dryness or wetness of the region at a varying time scale of short-term (1-month) to long-term (36-month) (Guttman, 1999). Additionally, several other climatic variables such as temperature, relative humidity, and evapotranspiration are also significant predictors of multiple drought events (Rhee and Im, 2017). The increasing temperature triggers the rate of evapotranspiration, leading to long-term hydrological and agricultural drought conditions (Bazrafshan, 2017; Jeong et al., 2014). Drought is a nonlinear phenomenon (Yang et al., 2018), and traditional methods have numerous limitations in dealing with the dynamics and nonlinearity inherent in the phenomenon. For instance, statistical methods are direct, simple, low-cost, and generalized but perform poorly in long-lag prediction because of their collinearity issues (Zhang et al., 2019). Additionally, statistical models fit poorly with nonlinear data and perform better for linear data analysis (Li et al., 2016). On contrary, Machine learning (ML) can model and forecast drought data using self-organizing and self-adaptive algorithms with nonlinear properties (Table 1) (Liu et al., 2018).

Machine learning algorithms are composed of instructions that enable them to acquire knowledge from historical data and formulate predictions without the need for extensive programming. Various ML methods such as Artificial Neural Network (ANN) (Dikshit et al., 2022; Fahimi et al., 2017), Support Vector machine (SVM) (Ganguli and Reddy, 2014), Decision Trees (DT), and Random Forest (RF) are being used in drought prediction studies (Table 1) (Fahimi et al., 2017; Rhee and Im, 2017). A bibliographic review analysis for keywords SPI, Machine learning, and climate projections revealed the utilization of machine and deep learning neural networks for drought predictions in the broad perspective of climate change (Fig. 1). Furthermore, ML applications are used for drought predictions in various regions like China (Zhang et al., 2019), USA (Agana and Homaifar, 2017; Park et al., 2016), northeast Asia (Rhee and Im, 2017), northeast Africa (Belayneh et al., 2016b), southeast Australia (Feng et al., 2019), etc. However, a few studies have been conducted in central Europe for ML-based drought predictions (Felsche and Ludwig, 2021; Forzieri et al., 2014; Li et al., 2021).

A rigorous review of previous studies also overlooked the testing of machine learning (ML) algorithms for future drought predictions in

Table 1
A review of drought predictions employing machine learning methods.

Region	Indicator	ML models	Findings	Reference
Pakistan	SPI	OP-ELM, DENFIS	DENFIS provided better accuracy for SPI-3, 6 and 9 predictions at three stations	Adnan et al., 2023
China	SPI	GPR	GPR blending with reanalysis products outperformed drought prediction compared to station-based SPI	He et al., 2023
Morocco	SPI	RSS, RF, M5P, REPTree	REPTree model outperformed other ML models for predicting short term (SPI-3 and SPI-6) droughts	Acharki et al., 2023
Algeria	SPI	SVM, additive regression (AR), BG, RSS, RF	SVM outperformed other models for SPI-3,6,9, and 12.	Achite et al., 2023
Central India	SPI	RF, RT, GPR	RF outperformed other models for SPI-6 and SPI-12	Elbeltagi et al., 2023a
India	SPI	(AR), random subspace (RSS), M5P, bagging	Bagging and M5P outperformed other models for SPI-3 and SPI-6 prediction.	Pande et al., 2023
Syria	SPI	BG, RSS, RT, and RF	BG & RF had the best performance	Mohammed et al., 2022
	SPEI	SVM, ANN, KNN	SVM algorithm was the best	Khan et al., 2020
Australia	SPEI	SVR	SVR is considerably efficient in predicting drought	Deo et al., 2018
Ethiopia	SPI	ANN, SVR	The SVR algorithm provided the best results.	Belayneh et al., 2016b

different temperature scenarios which need to be evaluated (Achite et al., 2022; Belayneh et al., 2016a; Djerbouai and Souag-Gamane, 2016; Nafii et al., 2023). In this context, our study aimed to forecast short-term drought (SPI-3) from different climatic predictors under historical (1901–2020) and future (2021–2100) climatic scenarios of SSP2-4.5 and SSP4-6.0 employing machine learning algorithms.

Specifically, we utilized four ML algorithms in three developed scenarios: ((SC1 (rainfall (R) + average monthly temperature (T) + daily mean maximum temperature (T_{max}) + daily mean minimum temperature (T_{min})), SC2 (R), and SC3 ($R + T$)) of climatic predictors for short-term drought forecasting (based on SPI-3) from historical and future projected climatic scenarios derived from the ensemble mean of three GCMs of CMIP6 in Hungary, Central Europe. Hence, our study used an approach of utilizing temperature as a predictor of short-term drought i.e., SPI-3 forecasting in the longer run. The output of this study suggested the best ML model performance for the best climatic scenario based on the specified evaluation parameters among the three climatic scenarios. The study also determined the closest and best SSP scenarios for future forecasting of SPI-3 at a regional scale. Hence, it will provide a useful future opportunity to utilize these ML algorithms in long-run drought forecasting and its impacts in other European regions.

2. Materials and methods

2.1. Study area

The area selected for the current study is Hungary, which lies between latitudes 45–48.5°N and longitudes 16.5–22.5°E in the Carpathian Basin of Central Europe (Fig. 2). Topographically, the country is mostly flat/plain area called 'Hungarian Great Plain' in the east of river Danube. A hilly region lies in the west of the Danube and Northern hills, with 'Mount Kekes' being the highest peak of the region located northeast of Budapest (Scranton, 2022; Vadas, 2022). Most of the country's elevation lies below 250 m. The region has a continental temperate climate with an average temperature ranging from −1 °C in winter to 22 °C in summer and well distributed average rainfall of 550 mm (Buzási, 2021; Vadas, 2022). The region is vulnerable to the detrimental effects of climate change and global warming (Csete and Barna, 2021). Like other European countries, it is affected by the increasing frequency of droughts leading to low crop yield and animal devastation (Ceglar et al., 2018; Harsányi et al., 2021). Generally, every 3rd to 4th year the region experiences low to moderate drought conditions in some parts of the region and is expected to rise further until the next century (Gálos et al., 2007). Hence, the climatic vulnerability of the region makes it significant to study and analyze drought prediction utilizing ML methods.

2.2. Data used

2.2.1. Historical observational dataset

Freely available dataset of four climatic variables rainfall (R) (mm), average monthly temperature (T) (°C), the daily maximum mean temperature in the month (T_{max}) (°C), and daily minimum mean temperature in the month (T_{min}) (°C) were collected from the National Meteorological Service of Hungary (https://www.met.hu/en/eghajlat/magyarorszag_eghajlata/eghajlati_adatsorok/, accessed on May 2022) for the historical baseline period of 1901–2020. Data were collected for three meteorological stations: Budapest (BD) (central Hungary), Szeged (SZ) (east south Hungary), and Szombathely (SZO) (west Hungary) (Fig. 2). The selected stations belong to varied topographical and agroecological regions of the country and prove to be a good representative to examine the short-term drought predictions for future

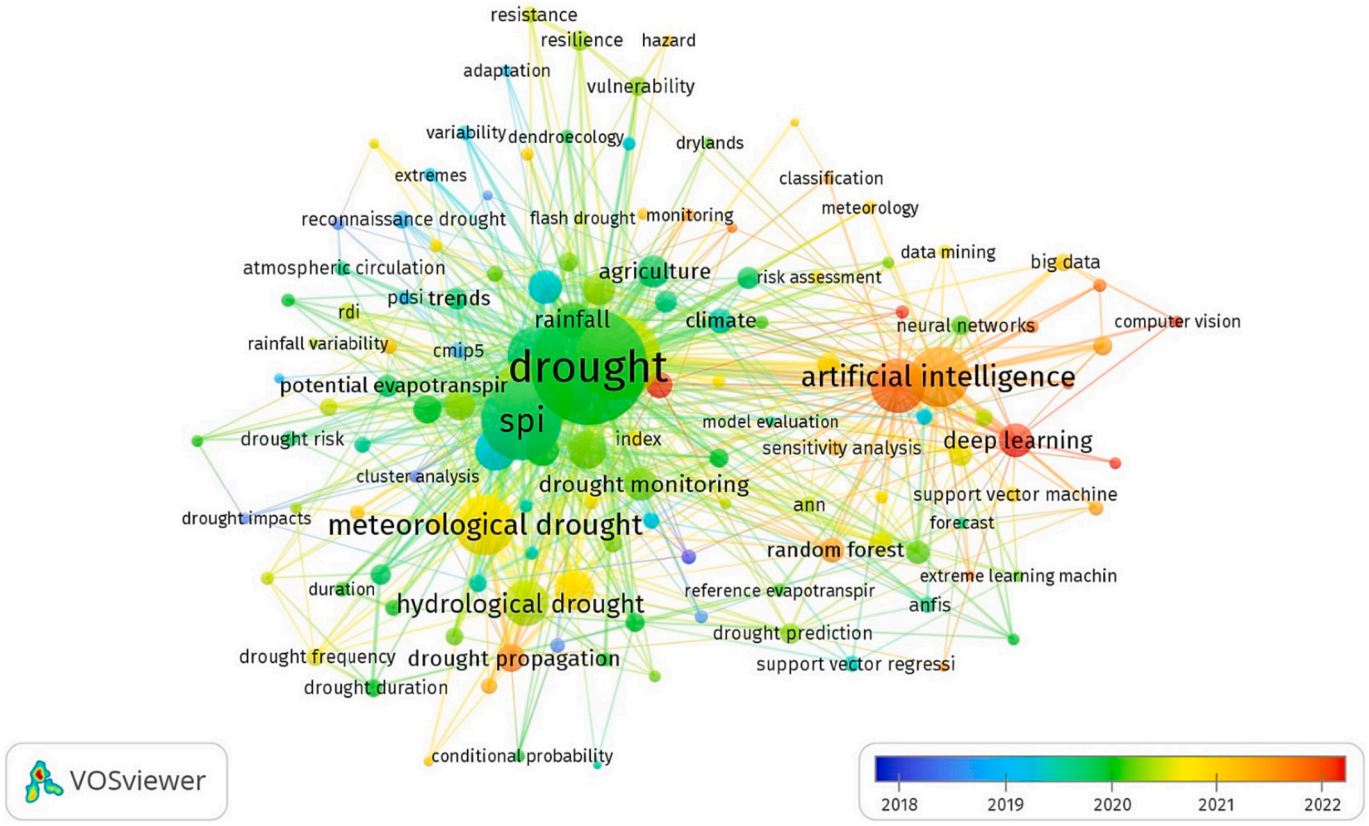

Fig. 1. A bibliographic analysis of machine learning based SPI drought predictions based on web of science core collection databased for the last ten years (n = 5531) indicating an increasing trend of using artificial intelligence in drought research (red color). (For interpretation of the references to color in this figure legend, the reader is referred to the web version of this article.)

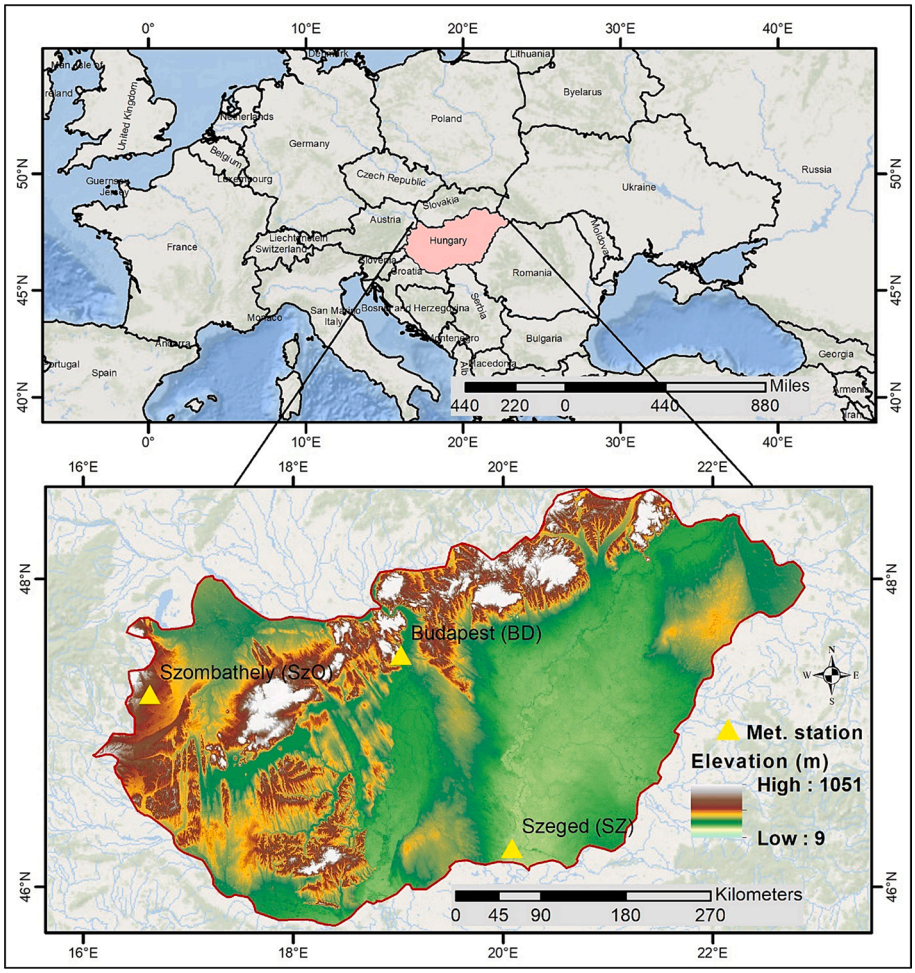

Fig. 2. Location of the study area and selected stations in Hungary, Central Europe.

implications of better hydrological strategies.

The descriptive statistics of all climatic variables are presented in Table A1 and their evolution is in Fig. 3.

2.2.2. Future projected dataset

The Coupled Model Intercomparison Project Phase 6 (CMIP6) is a research initiative aimed at improving our understanding of the Earth's climate system in the future and its response to external forcings, such as greenhouse gases, aerosols, and land use changes (Samantaray et al., 2022; Wang et al., 2021). The General circulation models (GCMs) of CMIP6 provide robust climatic projections compared with previous phases under different scenarios of socioeconomic pathways (SSPs) adopted to project future climatic extremes at global and regional scales (Hersi et al., 2023; Saha and Sateesh, 2022; Zhao et al., 2023). The CMIP6 GCMs are validated and reliable for replicating historical climate patterns and projecting future scenarios. Peer-reviewed studies confirm the robustness of CMIP6 models, supporting their use in climate research and impact assessments (Holtanova et al., 2023; Palmer et al., 2021; Pimonsree et al., 2023; Ullah et al., 2022). The CMIP6, organized by the World Climate Research Program (WCRP) provides climatic projections under four SSP scenarios (SSP1-2.6; sustainability, SSP2-4.5; middle of the road, SSP3-7.0; regional rivalry, SSP4-6.0; inequality, SSP5-8.5; fossil-fueled development) (O'Neill et al., 2016; Su et al., 2021). Our study used SSP2-4.5 (assuming a gradual transition to a sustainable future), and SSP4-6.0 (assuming a future with a high level of inequality and slow economic growth) to project future (2021–2100) climatic indicators (i.e., rainfall R, mean temperature T, maximum temperature T_{max}, and minimum temperature T_{min} from ensemble mean of three GCMs of CMIP6 presented with their characteristics in Table 2. Trends of future projected climatic indicators were analyzed in three defined periods: near future (NF) (2021–2040), mid-future (MF) (2041–2070), and far future (FF) (2071–2100).

2.3. Standardized precipitation index (SPI)

The SPI is a widely acknowledged meteorological drought index for drought assessment recommended by the World Meteorological Organization (WMO) at varying short (SPI-1 and SPI-3) and long (SPI-9 and SPI-12) time scales (Lotfirad et al., 2022; Yerdelen et al., 2021; Zeybekoğlu and Aktürk, 2021). It presents the deficit or excess of precipitation at a given location relative to its long-term mean, standard deviation, and fitting gamma distribution (Guttman, 1999). The SPI derived by normalizing the cumulative gamma distribution function (CDFs) of rainfall data can be expressed by Eq. (1):

$$g(x) = \frac{1}{B^{a}\hat{\Gamma}(a)} x^{a-1} e^{-x/B} \quad for \;\; x > 0 \tag{1}$$

where $g(x)$: gamma probability density function (pdf), x Rainfall, a: shape parameter ($a > 0$), B: scale parameter ($B > 0$), $\hat{\Gamma}(a)$: the gamma function. Short-term SPI (SPI-1 and SPI-3 months) values are best suited to describe the shallow soil moisture deficit of the location while long-term presents the hydrological reservoir of the region with long-term impacts (Zhao et al., 2023). We aimed to calculate and forecast the SPI-3 drought, reflecting the short-term seasonal water deficit changes

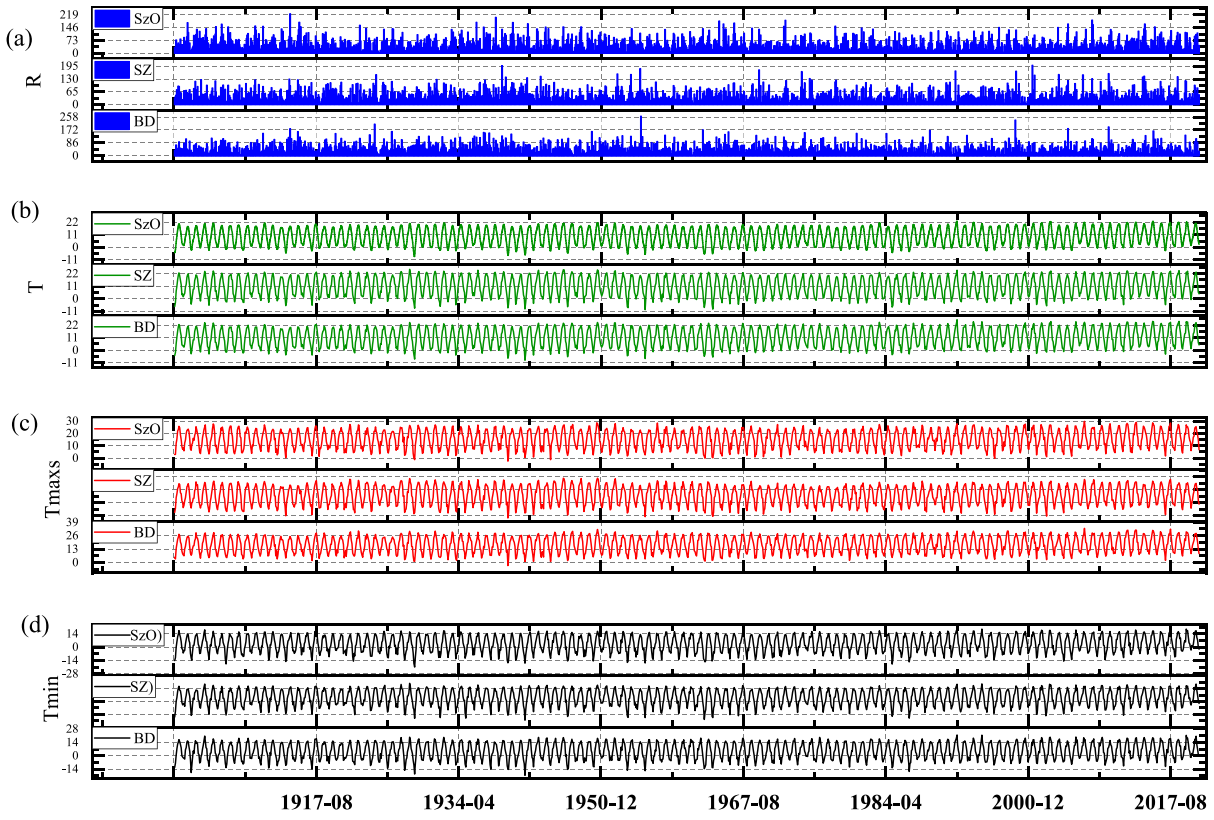

Fig. 3. An overview of the evolution of studied climate variables from 1901 to 2020 across Hungary: (a) rainfall (R) (mm), (b) average monthly temperature (T) (°C), (c) daily maximum mean temperature in the month (T_{max}) (°C), (d) daily minimum mean temperature in the month (T_{min}) (°C).

Table 2
Selected GCMs from CMIP6 used in the study.

Model Name	Country	Resolution	variant	Reference
CanESM5	Canada	2.8° × 2.8°	r1i1p1f1	Swart et al., 2019
MIROC6	Japan	1.4° × 1.4°	r1i1p1f1	Tatebe et al., 2019
MRI-ESM2-0	Japan	1.12° × 1.12°	r1i1p1f1	Kawai et al., 2019

over selected stations in Hungary from historical (station-based) and future (CMIP6) climatic perspectives. The output of SPI is recognized by positive and negative values, with a negative SPI value referring to the occurrence of drought following the severity thresholds in Table 3.

2.4. Trend analysis of present and future climatic variables and SPI drought index

The non-parametric Mann-Kendall (MK) trend test (Khanmohammadi et al., 2022; Xu et al., 2003) along with directional Theil Sen's slope (SS) estimator (Sen, 1968; Theil, 1950) was applied to all selected climatic variables i.e., (R), (T), (T_{max}), and (T_{min}) and SPI-3 for historical baseline (1901–2020) and projected in NF (2021–2040), MF (2041–2070), and FF (2071–2100) periods. The MK test assumes the null hypothesis H° (stating no significant trend in climate and SPI-3 drought over the longer run) and alternate hypothesis H1 (stating a significant trend in climate and SPI-3 drought over the longer run) at the significance level of $P < 0.05$, $p < 0.01$, and $p < 0.001$. The Sen's slope determines the positive (increasing) and negative (decreasing) magnitude of the climatic or drought trend. Further, to find the trend interrupting or changing points in long-term historical time series variables, the Buishand range (BR) test is applied which is based on the hypothesis of detecting mean shift in series presented by Eq. (2).

Table 3
SPI categories of drought intensity.

SPI values	Categories
−1 0.0 < SPI < −0.5	Mild drought
−1.49 < SPI < −1.0	Moderate drought
−2.0 < SPI < −1.5	Severe drought
SPI ≤ −2.0	Extreme drought

$$S_k = \sum_{i=1}^{k} (X_i - \overline{X}) \quad k = 1, 2, 3, \cdots\cdots n \tag{2}$$

where S_k is the rescaled partial sum of the series, X_i is the observed climatic indicators data series and $\overline{X}$ presents the mean of climatic indicators and $n = 120$ presents the total numbers in time series (Yuce et al., 2023). Moreover, the Box plot and Mann-Whitney test were applied to examine the distribution, range, and mean difference between the historical and projected climatic variables.

2.5. Machine learning methods for short term agricultural drought (SPI-3) prediction

ML provides potentially viable algorithms for analyzing complex environmental phenomena, such as natural hazards and risk assessment (Deo et al., 2017; Mohammed et al., 2022), and has also been widely used to predict and forecast drought assessment in recent decades (Dayal et al., 2017; Deo et al., 2018; Felsche and Ludwig, 2021). Better model performance and big data handling make ML a popular and feasible choice compared to traditional statistical approaches in drought prediction studies. Thus, keeping in view the significance of ML and achieving high accuracy in drought prediction, we focused on applying rule-based Decision Table (DT) and ensemble tree-based Bagging (BG), Random Forest (RF), and M5P. The rule-based system of DT facilitates straightforward and easy interpretation and is easier to handle

compared to the hierarchical architecture of tree-based algorithms (Gao et al., 2019). Moreover, M5P is based on the essence of decision trees incorporating linear regression at leaves. Hence, making it suitable to capture both linear and non-linear relationships proving it to be a more flexible approach to be used in drought prediction studies (Acharki et al., 2023; Pande et al., 2023). Furthermore, the ensemble nature of BG and RF aggregating the predictions of multiple decision trees proves them to be robust and accurate for drought predictions (Elbeltagi et al., 2023a; Mohammed et al., 2022). Hence, the selected ML algorithms are described below in detail.

2.5.1. Bagging (BG)

The bagging, also known as bootstrap aggregation developed by Breiman (1996) is an ensemble machine learning method that combines multiple regression trees to enhance the predictive performance. It creates several random subsets (B) of the training data through the bootstrap sampling method, and each subset is used to train individual regression models (Breiman, 1996). Finally, the predictions are aggregated by the average output of all models. It is presented by Eq. (3).

$$\widehat{f}_{bag}(x) = \frac{1}{B}\sum_{b=1}^{B}\widehat{f}^{*}b(x) \tag{3}$$

where B are the models trained on bth bootstrapped samples and $\widehat{f}_{bag}(x)$ is the final average of all prediction models. This model has been widely used in hydrological and drought forecasting research because of its better prediction capacity (Achite et al., 2023; Saha et al., 2021; Zounemat-Kermani et al., 2021). We used this model because it can fabricate the decision tree using different subsets and assemble them in the final model (Arabameri et al., 2022). This model can improve alignment accuracy by reducing the discrepancy in alignment error (Breiman, 1996). The parameters selected for bagging are listed in Table 4.

2.5.2. Random Forest (RF)

The Random Forest (RF) is a non-parametric ensemble bagging method that uses a supervised learning technique for prediction and classification purposes (Arabameri et al., 2022; Breiman, 2001). Random forest is a tree-based ensemble machine learning algorithm that uses several decision trees as base learners where each tree is created from a bootstrap random sample with replacement from training input. The procedure reduces variance and overfitting and improves the accuracy of the model output (Arshad et al., 2023a). Hence, various numbers of predictor variables are connected to the nodes of the tree, and a random number of data points are selected from the dataset to build the model. The final predictions were the average of all predictions from all decision trees (Leo et al., 2021; Zounemat-Kermani et al., 2021). Overall, Model performance is highly dependent on the optimization of variables (Ganguli and Reddy, 2014). Currently, we use a 'Random Tree Classifier' to produce decision trees with no depth limits. Random splits were performed to reduce the variance in the target class. The model parameters are listed in Table 4.

Table 4
Parameters selection of applied ML algorithms.

ML Algorithms	Parameters
Bagging	Base learner = weka.classifiers.trees.REPTree -M 2 -V 0.001 -N 3 -S 1 -L −1 -I 0.0, pool size P = 100, iterations = 10, random seed S = 1, num-slot = 1,
Random Forest	Algorithm = weka.classifiers.trees.RandomForest, radom seed S = 1, ntrees I = 100, max tree depth = 0, batch-size = 100, iterations = 100, variance V = 0.001, classifier capabilities = −do-not-check-capabilities
M5P	weka.classifiers.trees.M5P -M 4.0 -num-decimal-places 4, Batch size = 100
Decision Table	weka.classifiers.rules.DecisionTable, Rules = 10, search method S = Best first, Search direction = forward, cross-validation CV = leave one out

2.5.3. M5P

The M5P algorithm was proposed by Quinlan (1992) which uses a regression tree for predictions. The M5P model integrates linear regression function at the leaf nodes, and it is also used to develop a tree model. The regression tree is based on the following elements: root node (dataset/database), internal node (condition or logic on the dataset), and leaf node (regression model on values of a dataset) (Granata and Di Nunno, 2021). The M5P process is based on pruning, evacuation, and substitution of trees which eventually build a tree model. The model is usually used to predict the output based on various input datasets (Quinlan, 1992). The M5P regressor determines the splitting criteria for its model tree based on the calculation of errors at each node. The error is evaluated by analyzing the standard deviation of the class values reaching a node. At each node, the attribute that offers the maximum expected reduction in error from testing each attribute is selected for splitting. The standard deviation reduction (SDR) Eq. (4) is used to minimize the expected error (Sihag et al., 2019).

$$SDR = sd(K) - \sum\frac{|K_i|}{|K|} \times sd(K_i) \tag{4}$$

where K_i presents the instances from K_1, K_2, K_3……. sd is the standard deviation. The selected parameters are presented in Table 4.

2.5.4. Decision Table (DT)

The DT (Kohavi, 1995) stands for a sophisticated, scheme-specific learning algorithm (Pham et al., 2022). The DT builds using classes and employs a straightforward decision table majority classifier (Chen, 2016). This algorithm can handle different types of data such as numeric, date, and nominal (Kohavi, 1995). The DT has two different parts: the first one represents features listed in the table, while the second is a body of DT which is made up of labeled instances from the space of schema (Huang et al., 2022).

2.6. Modelling methodology

To assess the performance capability of ML algorithms in forecasting the short-term drought SPI-3, we added temperature T, T_{max}, and T_{min} and R as input variables in three combination scenarios (Table 5).

Further, to forecast and predict the short-term drought SPI-3 from input variables, BD located in central Hungary is chosen as a leading station, where all mentioned scenarios in Table 5 (SC1, SC2, SC3) and ML-algorithms (BG, DT, M5P, RF) were implemented on the historical dataset only i.e., 1901–2020 to find out the best scenario and highest performed ML algorithm based on the evaluation metrics. For the model's implementation, the historical dataset arranged in monthly columns of all input and output variables (n = 1440) is randomly split into training (TR) (70 %, n = 864), testing (TS) (15 %, n = 288) and cross-validation (CV) (15 %, n = 288). The process was followed by the implementation of the best selected scenario and ML algorithm on the rest stations namely Szeged (SZ) and Szombathely (SZO) in the southeast and western parts of the region. The selected scenarios and algorithm were implemented to forecast the SPI-3 from historical to projected (2021–2100) dataset derived from the ensemble mean of three GCMs of

Table 5
Scenarios developed for ML-based drought prediction using SPI-3.

Scenarios	Input	Component	Output
SC1	$R + T + T_{max} + T_{min}$	Rainfall (monthly) + temperature (daily + monthly)	SPI-3
SC2	R	Rainfall (monthly)	SPI-3
SC3	$R + T$	Rainfall (monthly) + temperature (monthly)	SPI-3

CMIP6 under two climatic scenarios i.e., SSP245 and SSP4-6.0. This process was conducted in the Weka environment (V.3.9.5), as recommended, and utilized in recent research (Elbeltagi et al., 2023b; Lin et al., 2021; Mohammed et al., 2022). The initial settings were bag-size (100), batch-size (100), num-Iteration (100), and random seed (1) (Table 4). The detailed steps of the whole research are presented in the methodology framework (Fig. 4).

2.7. ML-algorithms performance evaluation

To evaluate the performance of ML-algorithms, five statistical indicators were used. These include Nash-Sutcliffe efficiency (NSE), root mean squared error (RMSE), mean absolute error (MAEr), correlation coefficient (*r*), and index of agreement (DAg), presented in Table 6. Moreover, a Tylor diagram was employed to check the prediction performance accuracy of four ML algorithms (BG, DT, M5P, RF) (Taylor, 2001).

3. Results

3.1. Variability of historical and projected climatic variables (rainfall and temperature) in different SSP scenarios

Exploratory analysis of historical (1901–2020) (HS) and projected (2021–2100) (SSPs) datasets of rainfall and temperature, as presented in Figs. 5 and 6, reveals an increasing trend for both variables. The Mann-Whitney analysis showed the mean historical rain was to be around 535 (SZ)–632 (SZO) mm for the three stations while the mean projected rain

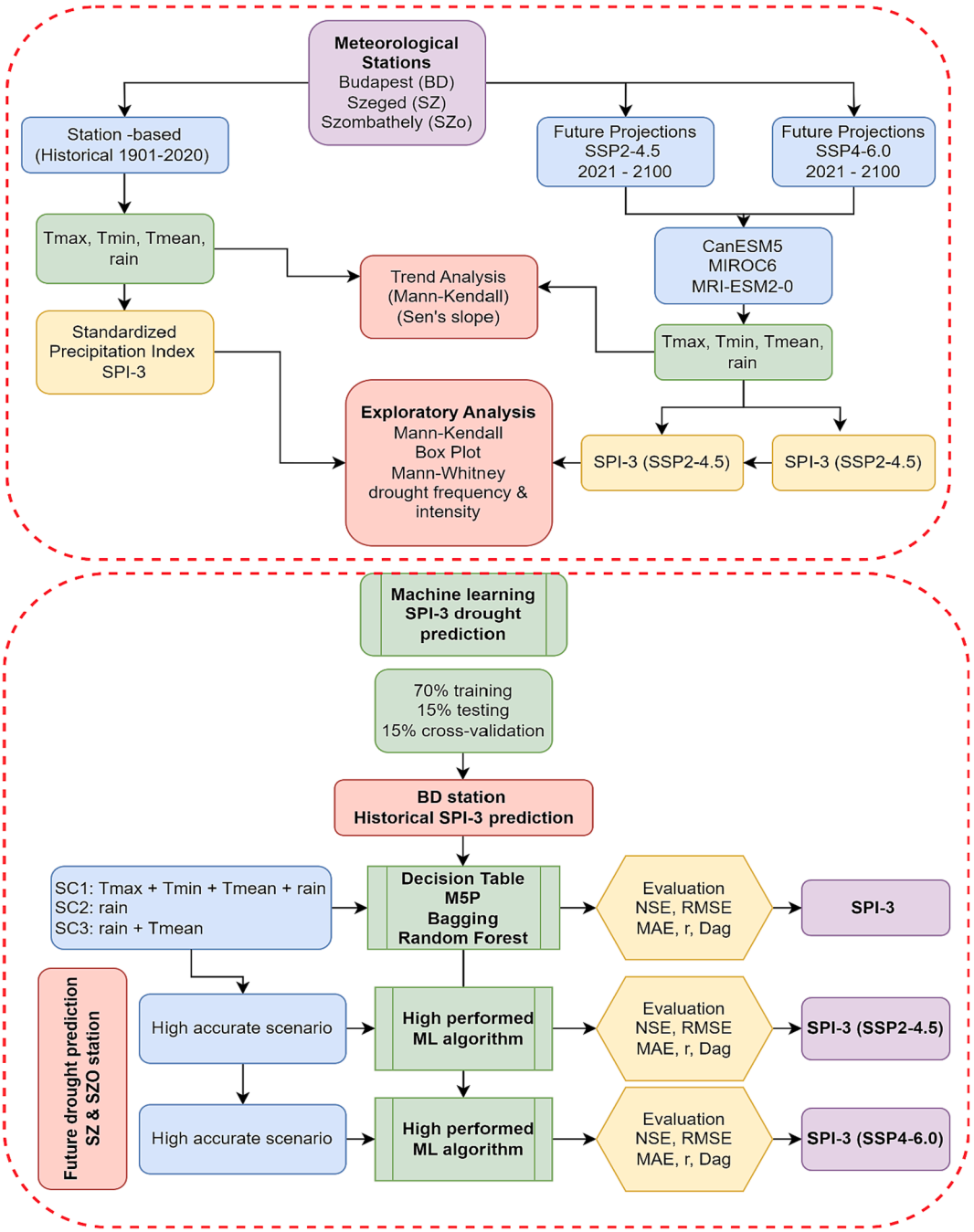

Fig 4. Methodology Framework.

Table 6
Performance evaluation metrics of machine learning algorithms used.

Index	Equation*	Range	Best agreement	Reference
NSE	$NSE = 1 - \frac{\sum_{i=1}^{n}(SPI_{Prd} - SPI_{Cal})^2}{\sum_{t=1}^{n}(SPI_{Cal} - \overline{SPI_{Cal}})^2}$	[−∞_1]	1	(Nash and Sutcliffe, 1970)
RMSE	$\mathrm{RMSE} = \sqrt{\frac{1}{N}\sum_{i=1}^{N}(SPI_{Cal} - SPI_{Prd})^2}$	[0_+∞]	0	(Willmott et al., 1985)
MAEr	$MAEr = \frac{1}{N}\sum_{i=1}^{N}\lvert SPI_{Prd} - SPI_{Cal}\rvert$	[0_+∞]	0	(Hauduc et al., 2015; Willmott et al., 1985)
r	$r = \left[\frac{\sum_{i=1}^{n}\{(SPI_{Cal} - \overline{SPI_{Cal}})(SPI_{Prd} - \overline{SPI_{Prd}})\}}{\sqrt{\sum_{i=1}^{n}(SPI_{Cal} - \overline{SPI_{Cal}})^2}\sqrt{\sum_{i=1}^{n}(SPI_{Prd} - \overline{SPI_{Prd}})^2}}\right]$	[−1_+1]	+1	(Pearson and Henrici, 1896)
Dag	$DAg = 1 - \frac{\sum_{i=1}^{n}(SPI_{Cal} - SPI_{Prd})^2}{\sum_{i=1}^{n}(\lvert SPI_{Prd} - \overline{SPI_{Cal}}\rvert + \lvert SPI_{Cal} - \overline{SPI_{Cal}}\rvert)^2}$	[0_+1]	+1	(Hauduc et al., 2015; Willmott et al., 1985)

* SPI_{Cal}: calculated *SPI* value based on Eq. (1); SPI_{Prd}: predicted value from ML-algorithms (BG, DT, M5P, RF); $\overline{SPI_{Cal}}$: average of calculated values; $\overline{SPI_{Prd}}$: average of predicted values.

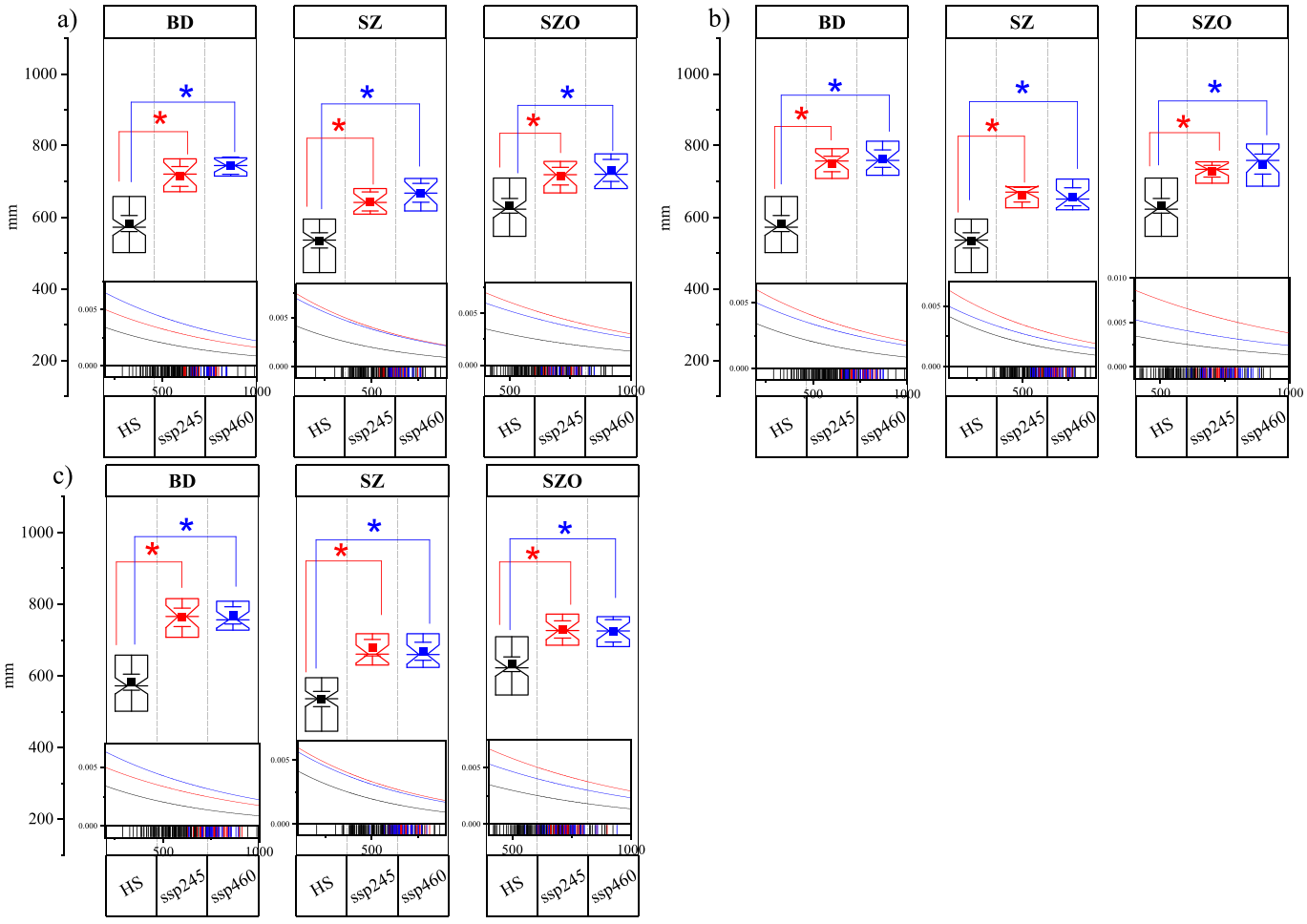

Fig. 5. Notched box plot, exponential distribution (lower part), and Mann-Whitney (represented by ⋆) based comparative mean of projected yearly rainfall under historical (HS), SSP245, and SSP460climatic scenarios for three stations: (a) NF (2021–2040), (b) MF (2041–2070), (c) (2071–2100), □ mean, whisker range: confidence interval, whisker probability (%): 95 %, ⋆: $p < 0.05$.

under SSP245 and SSP460 exceeded 600 mm in NF (2021–2040) which further increased to around 700 mm for BD station in MF with less increase at SZ and SZO station (Fig. 5). Moreover, the exponential distribution indicates that the highest increase in rainfall was projected during the MF (2041–2070) and FF (2071–2100) under the ssp245. Statistically, the Mann-Whitney *U* test revealed a significant difference between the distributions of the HS data and the projected one (Fig. 5).

Also, the average temperature was projected to be increased in the target stations (Fig. 6). The average temperature for the HS data ranged from 9.6 °C in SZO to 11.39 °C in BD. Under different climate scenarios, this is projected to be increased to reach 17 °C and 19 °C. The exponential distribution shows a clear shift in projected temperature during the MF (2041–2070), blue line), and FF (2071–2100), blue line). More global warming is expected under SSP460 in the near and mid-future (2021–2070) (Fig. 6). In this context, the Mann-Whitney *U* test revealed a significant difference between the distributions of the HS

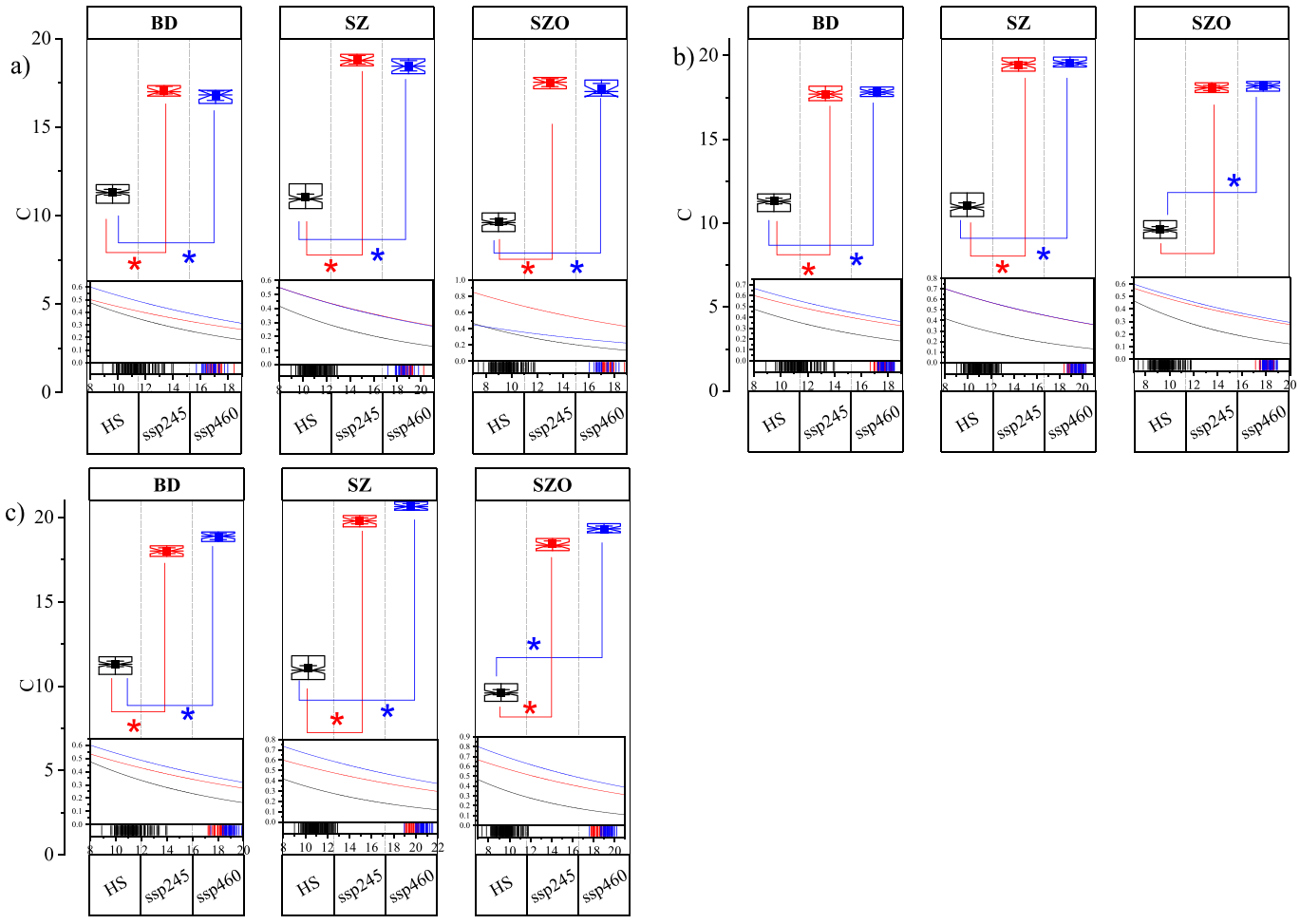

Fig 6. Notched box plot, exponential distribution (lower part), Mann-Whitney (represented by ⋆) based comparative mean of projected monthly temperature under historical, SSP245, and SSP460climatic scenarios for three stations: (a) NF (2021–2040), (b) MF (2041–2070), (c) (2071–2100), □ mean, whisker range: confidence interval, whisker probability (%): 95 %, ⋆: $p < 0.05$.

temperature data and projected one at the three stations under SSP245 and SSP460 (Fig. 6).

3.2. Trend analysis of climatic & short-term agricultural drought events (1900–2100)

Mann-Kendall trend and Sen's slope analysis of historical (1901–2020) climatic variables revealed a significant ($p < 0.001$, $p < 0.01$) declining trend of rainfall *R* with Sen's slope = −1.01, −0.75, and −0.50 at BD, SZO and SZ stations (Table A2). Historical T_{max} and T_{min} revealed a significant ($p < 0.05$, $p < 0.01$, $p < 0.001$) increasing trend at three stations. Projected T_{min} under SSP2 exposed a significant ($p < 0.05$, $p < 0.01$) rising trend in MF (2041–2070) at three stations and FF (2071–2100) at SZ and SZO stations. Projected T_{max} and T_{min} under SSP4 scenario exposed significantly ($p < 0.05$, $p < 0.01$, $p < 0.001$) more increasing trend in NF (2021–2040) and MF (2041–2070) of three stations and FF (2071–2100) at SZO station. Overall, **SSP4 revealed an increasing trend towards projected warming in central Europe than SSP2**. Hence, more droughts can be predicted under SSP4 (Table A2). The trend analysis of historical (1901–2020) short-term (SPI-3) droughts revealed a significant ($p < 0.05$, $p < 0.01$, $p < 0.001$) decreasing trend in SPI values (increase of droughts) with tau −0.12, −0.16, and −0.2, and Sen's slope −0.03, −0.04, −0.05 respectively at Szeged (SZ), Szombathely (SZO), and Budapest (BD) stations of the region. Frequently decreasing SPI values are observed after 1970 revealing an increasing trend of short-term drought at BD station from 1970 to 2020. At SZO station, the year 1966 is identified as a trend breaking year with increasing SPI values after 1966. Further, projected SPI-3 revealed an increasing trend of short-term droughts in NF (2021–2040) with tau = −0.12 (BD, SSP2), −0.13 (SZ, SSP2), −0.08 (SZO, SSp2), −0.1 (BD, SZ, SSP4), and −0.2 (SZO, SSP4) **(**Table 7**).**

3.3. Intensity of historical and projected agricultural drought events

This study focused on calculating short-term drought prediction through negative SPI values i.e., less than −1. By tracking the drought events at the three studied stations, the following years/months can be distinguished as driest one: 01/01/1925 (SPI < −3, extreme drought), 10/01/1947 (SPI < −2, extreme drought), 04/01/1949 (SPI < −2, extreme drought), 07/01/1950 (SPI < −2, extreme drought), 07/01/2000 (SPI < −2, extreme drought), 06/01/2003 (SPI < −2, extreme drought), and 08/01/2013 (SPI < −1, Moderate drought) (Fig. 7). Moreover, drought events were found to be more frequent in the last few decades (Fig. 7). For SZO station, the frequency of drought categories can be divided into: [−4.19_−2.69, extreme drought] with 7 events, [−2.69_−1.87, severe drought] with 37 events, and [−1.87_−1.12, moderate drought] with 152 events (Fig. 7). For SZ station, 213 events were recorded for SPI ranged between −0.7 and −1.42 (normal to moderate drought), 81 events between moderate and severe drought [−2.08_−1.4], and 31 events as an extreme one (Fig. 7). For BD, the SPI captured 48 drought events ranging between extreme and severe drought [−3.29_−1.94], 94 events between −1.94 and −1.271

Table 7
Mann-Kendall trend and Sen's slope analysis of historical (1901–2020) and projected in near future (NF) (2021–2040), middle future (MF) (2041–2070), and far future (FF) (2071–2100) SPI-3 droughts under SSP2 and SSP4 scenarios at three stations (BD, SZ, and SZO) in Hungary, Cental Europe.

Station	SSP2-4.5					SSP4-6.0			
	var	Tau	P-value	Sen's slope	BR	Tau	P-value	Sen's slope	BR
BD	**SPI-3 (His)**	**−0.2**	**>0.001**	**−0.05**	**1970**	**−0.2**	**>0.001**	**−0.05**	**1970**
	SPI-3 (NF)	**−0.12**	0.4	**−0.09**		**−0.1**	0.5	**−0.08**	
	SPI-3 (MF)	0.2	0.1	0.16		0.18	0.16	0.19	
	SPI-3 (FF)	0.16	0.2	0.17		0.12	0.3	0.13	
SZ	**SPI-3(his)**	**−0.12**	**>0.05**	**−0.03**	**1944**	**−0.12**	**>0.05**	**−0.03**	**1944**
	SPI-3 (NF)	**−0.13**	0.4	**−0.15**		**−0.1**	0.2	**−0.18**	
	SPI-3 (MF)	0.12	0.3	0.10		0.18	0.15	0.18	
	SPI-3 (FF)	0.05	0.6	0.04		**−0.03**	0.80	**−0.02**	
SZO	**SPI-3 (His)**	**−0.16**	**>0.01**	**−0.04**	**1966**	**−0.16**	**>0.01**	**−0.04**	**1966**
	SPI-3 (NF)	**−0.08**	0.6	**−0.12**		**−0.2**	0.1	**−0.3**	
	SPI-3 (MF)	0.14	0.2	0.08		0.10	0.4	0.09	
	SPI-3 (FF)	0.11	0.3	0.10		0.02	0.8	0.03	

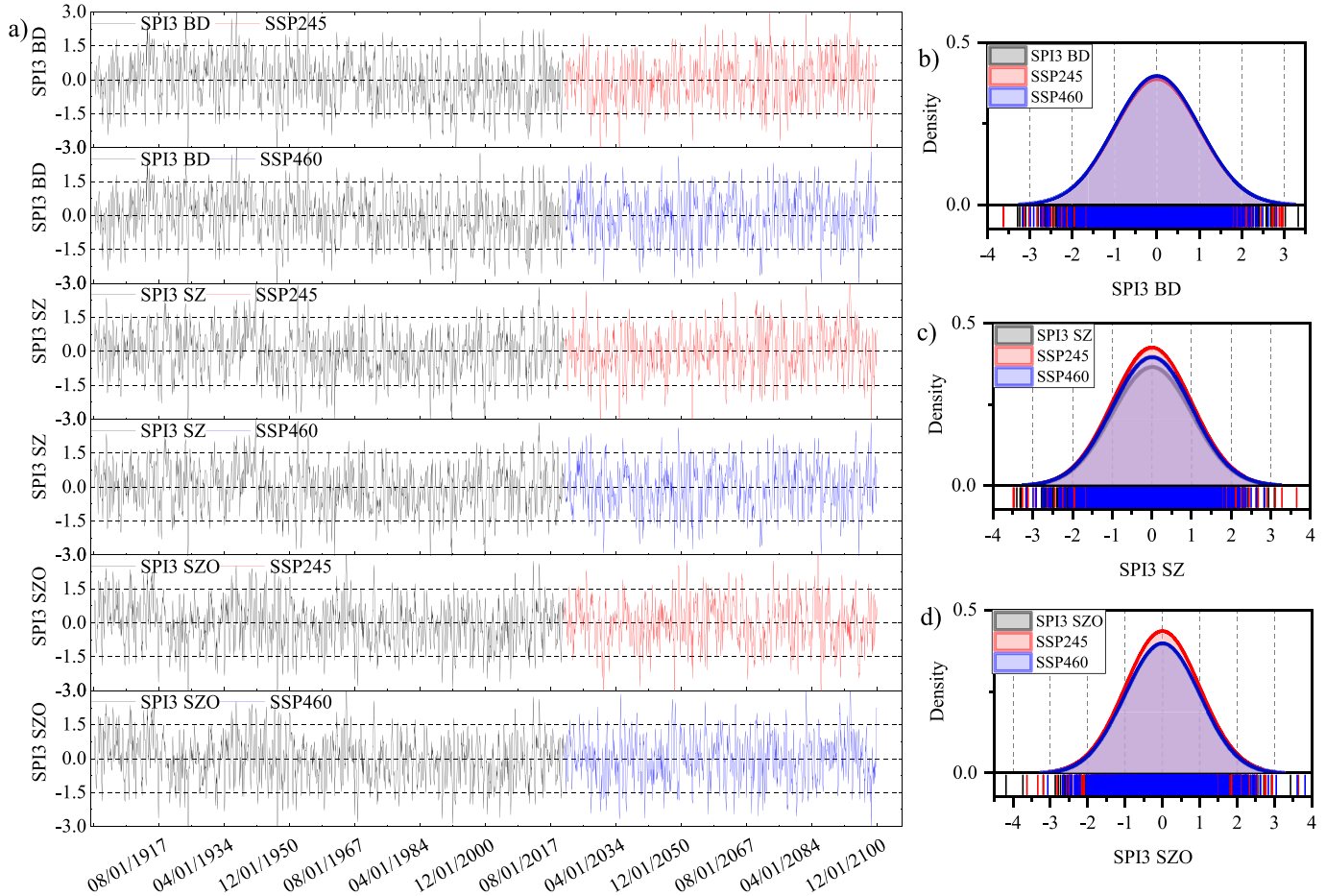

Fig. 7. (a) temporal evolution of drought events (SPI-3) within three stations across Hungary based on HS (1901–2020) and SSPs (2021–2100) along with normal distribution of the events (b: BD, c: SZ, d: SZO).

(moderate to severe drought), while 215 events were recorded as moderate to normal drought.

For projected drought events under the ssp2-4.5 the years 2028, 2030, 2031, and 2034 are identified with severe to extreme drought events in NF (2021–2040) with the following prominent months: 04 /01/2030, 05 /01/2030, and 03/01/2035, 07/01/2099 (SPI < −3, extreme drought), 10/01/2031, 02/01/2035, 04/01/2035, and 03/01/2076 (SPI < −2, extreme drought). More frequent severe to extreme droughts are identified in the NF scenario, while fewer drought events are identified at the end of the 21st century. Further, droughts identification under ssp460 also revealed 2028, 2029, 2032–34, 2040, 2049, and 2096 as severe to extreme drought years with following prominent months: 03/01/2028, 02/01/2031, 03/01/2031, 04/01/2040, 05/01/2040, 04/01/2049, 02/01/2060, 10/01/2091, 04,05, and 06/01/2096

(SPI < −2, extreme drought). Overall, more frequent droughts are projected under ssp4-6.0 (Fig. 7).

3.4. Efficiency of ML algorithms for drought (SPI-3) prediction at BD station

The performance of the ML was evaluated based on the three selected scenarios in Table 4. In the training stage the performance of SC1 ($R + T + T_{max} + T_{min}$) and SC3 ($R + T$) was superior to SC2 ($R$) (Fig. 8a, b, Fig. 9a, Table A3). However, in the cross-validation and testing stages, the SC3 had the best performance as compared to other scenarios (Fig. 8, Fig. 9). The ML (BG, DT, M5P, RF) algorithms varied in their ability to predict SPI-3 values. For the first scenario (SC1), the RF was able to predict the SPI-3 more accurately than other algorithms (Figs. 8–10) in the training (TR) stage. In this sense, the NSE-TR $_{RFSC1}$ was 0.89 (Fig. 9a), NSE- CrV $_{RFSC1}$ was 0.16 (Fig. 9b), and NSE- TS $_{RFSC1}$ was 0.21 (Fig. 9c) (Table A3). The RMSE ranged between 0.32 (TR, Fig. 9a), and 0.88 (TS, Fig. 9c). Interestingly, the correlation between SPI-3 and predicted values was 0.96 and 0.76 for RF and BG algorithms (TR, Fig. 8a, Fig. 9a), which decreased to 0.48 and 0.52 in the TS stage (Fig. 8f, Fig. 9c). Overall, based on the output of the TS stage of the SC1 and Tylor diagram, the ML performance can be classified as follows M5PSC1 > DTSC1 > BGSC1 > RFSC1 (Fig. 10a, d, g).

For the second scenario (SC2), in the **TR stage**, the **RF** was able to predict the SPI-3 more accurately than other algorithms ($DAg_{RFSC2\text{-}TR}$ = 0.89, $r_{RFSC2\text{-}TR}$ = **0.83**, $MEAr_{RFSC2\text{-}TR}$ = 0.43), followed by **BG** ($DAg_{BGSC2\text{-}TR}$ = 0.77, $r_{BGSC2\text{-}TR}$ = **0.7**, $MEAr_{BGSC2\text{-}TR}$ = 0.57), then **M5P** ($DAg_{M5P\ SC2\text{-}TR}$ = 0.67, $r_{M5P\ SC2\text{-}TR}$ = **0.76**, $MEAr_{M5P\ SC2\text{-}TR}$ = 0.66) (Fig. 6a, 7a, 8d, 9a). In the CV stage, the performance of the RF algorithm ($DAg_{RFSC2\text{-}CV}$ = 0.56, $r_{RFSC2\text{-}CV}$ = 0.41, $MEAr_{RFSC2\text{-}CV}$ = 0.77) declines in favor of M5P ($DAg_{M5PSC2\text{-}CV}$ = 0.63, $r_{M5PSC2\text{-}CV}$ = 0.53, $MEAr_{M5PSC2\text{-}CV}$ = 0.65). However, in the TS stage, the M5P remained the best algorithm in predicting SPI-3 ($NSE_{M5PSC2\text{-}TS}$ = 0.33, $RMSE_{M5PSC2\text{-}TS}$ = **0.81**, $DAg_{M5PSC2\text{-}TS}$ = 0.66, $r_{M5PSC2\text{-}TS}$ = 0.58, $MEAr_{RFSC2\text{-}TS}$ = 0.65) (Fig. 9) (Table A3). Overall, based on the output of the TS stage of the SC2 and Tylor diagram, the ML performance can be classified as follow M5PSC2 > DTSC2 > BGSC2 > RFSC2 (Fig. 10b, e, h).

The third scenario (SC3) represents a relationship between monthly rainfall (R) and average monthly temperature (T). In this scenario, the RF showed high accuracy in predicting the SPI-3 values in all stages (TR, CV, TS). In the TR stage, the highest NSE value (0.89) and lowest RMSE (0.33) were recorded within the output of the RF algorithm, followed by BG output. Similarly, within the TS stage, the output from the RF algorithm (i.e., $NSE_{RFSC3\text{-}TS}$ = 0.88, $RMSE_{RFSC3\text{-}TS}$ = 0.33, $DAg_{RFSC3\text{-}TS}$ = 0.96, $r_{RFSC3\text{-}TS}$ = 0.96, $MAEr_{RFSC3\text{-}TS}$ = 0.27) was better than the other one (Fig. 9) (Table A3). In all stages the ML algorithms' performance can be ranked as: RFSC3 > BGSC3 > M5PSC3 > DTSC3.

To capture the best algorithms and the perfect combination between climate variables (i.e., scenarios) for predicting SPI-3, all output (predicted values) were plotted against observed SPI-3 by using a Tylor diagram. Fig. 11 revealed that in the training stage, RF-SC1 and RF-SC3 had the best performance followed by RF-SC2 and BG-SC1. In the CV stage, RF-SC3 had the best performance followed by BG-SC3 (Fig. 11). Finally, in the TS phase RF-SC3 was found to be superior to the other algorithms (Fig. 11). Based on the findings in this section, the RF-SC3 was used to validate its ability in predicting SPI-3 in the other two

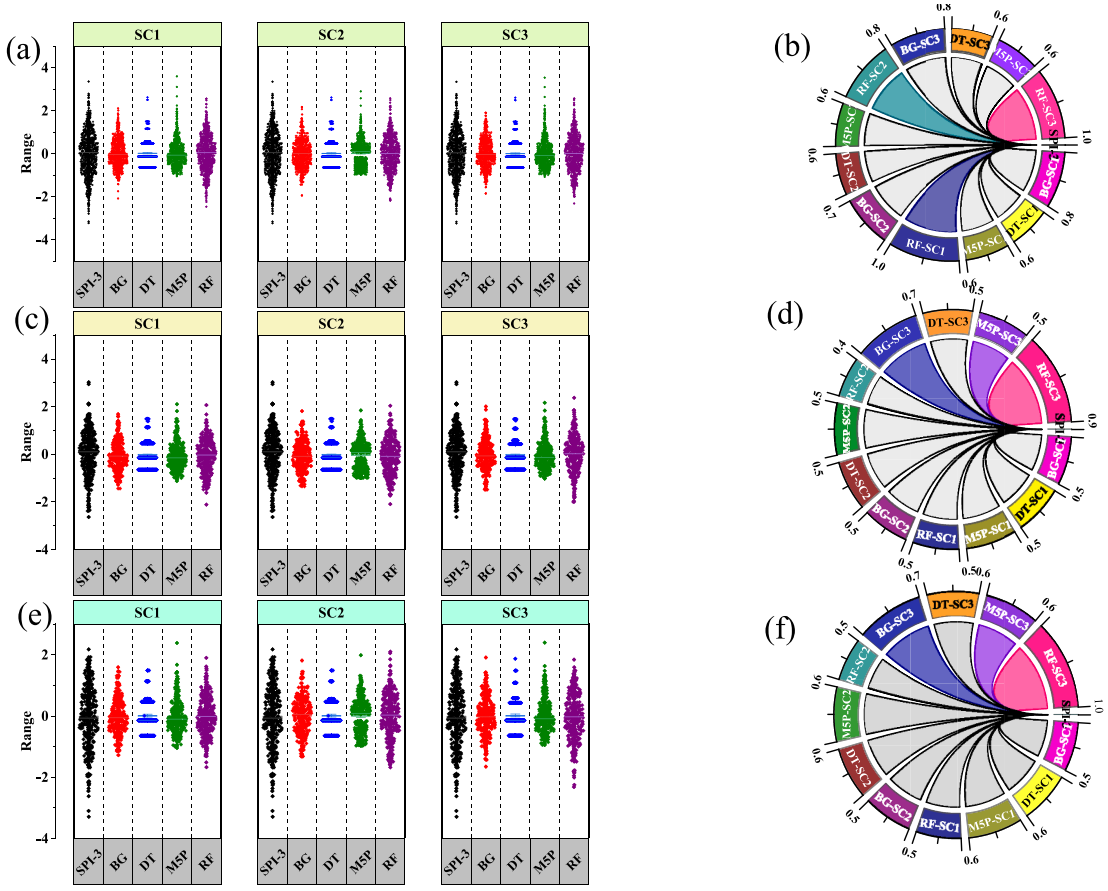

Fig. 8. Boxplot of observed and predicted SPI-3 by ML (BG, DT, M5P, RF) for three studied scenarios (SC1: $R + T + T_{max} + T_{min}$ SC2: R, SC3: $R + T$) in Budapest (BD) station: (a) training phase, (b) correlation matrix for trained data between observed SPI-3 and predicted SPI-3 based on chord diagram, (c) cross-validation phase, (d) correlation matrix for cross-validated data between observed SPI-3 and predicted SPI-3 based on chord diagram, (e) testing phase, and (f) correlation matrix for tested data between observed SPI-3 and predicted SPI-3 based on the chord diagram.

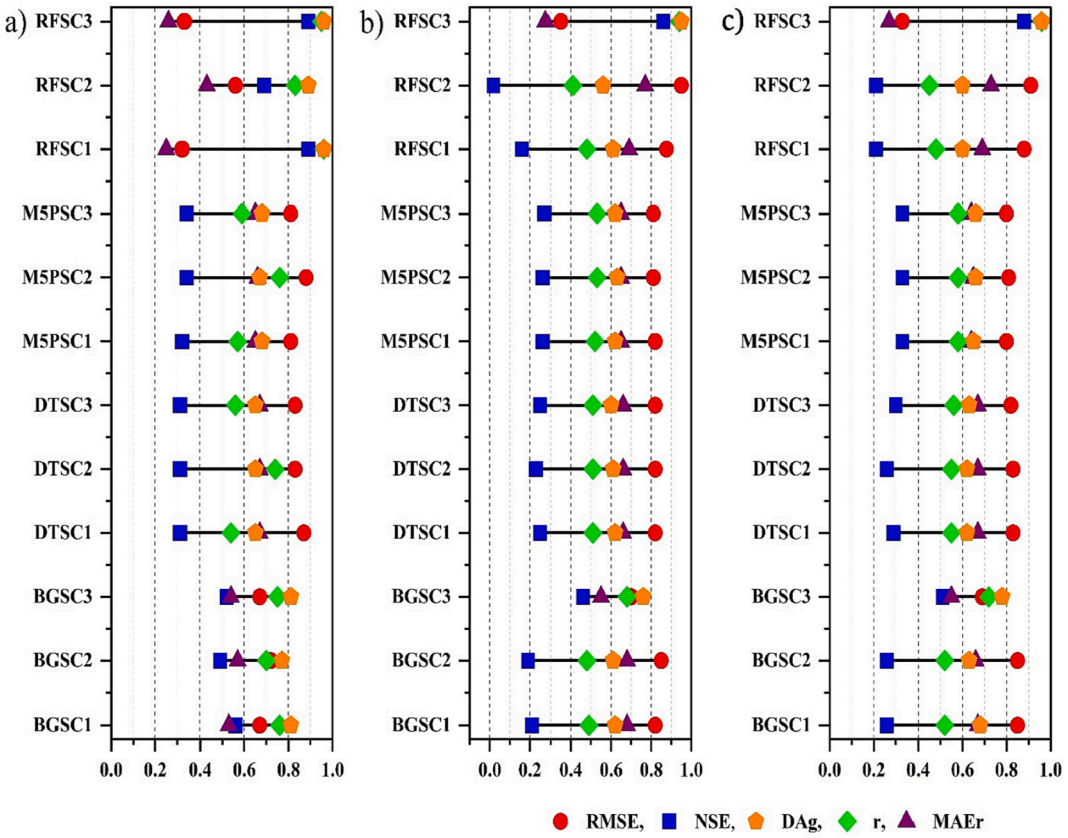

Fig. 9. Accuracy of ML (BG, DT, M5P, RF) algorithms in predicting SPI-3 values based on statistical indices (RMSE, NSE, Dag, r, MAEr) for studied scenarios (SC1 (R + T+ T_{max} + T_{min}), SC2 (R), and SC3 (R + T)): (a) training (TR), (b) cross-validation (CrV), (c) testing (TS).

selected stations namely SZO and SZ.

3.5. Implementation of RF-SC3 for future drought (SPI-3) forecasting at SzO and SZ

Further, to forecast the SPI-3 drought under future climatic scenarios, the best performed RF-SC3 is implemented at the two remaining SzO and SZ stations.

The evaluation metrics showed that the RF-SC3 forecasted the SPI-3 drought with high performance under SSP2-4.5 at both SZ and SzO stations. At SZ station, more accurate droughts were predicted in SSP2-4.5 scenario with RMSE = 0.346, r = 0.9569, NSE = 0.880, and DAg = 0.960 compared to SSP4-6.0 with RMSE = 0.379, NSE = 0.856, and DAg = 0.949. Similarly, at SzO station, accurate droughts were predicted in SSP2-4.5 scenario with RMSE = 0.347, r = 0.955, NSE = 0.879.

The actual SPI-3 was calculated and treated as observed data and plotted against the predicted data by RF-SC3 in both SZO and SZ. The boxplot showed that predicted and observed data had almost the same average, however, the range of observed data was wider than the predicted one (Fig. 12).

Fig. 13 represents the temporal evolution of drought events, based on the calculated SPI-3 (HS + SSPs) and the predicted one (SC3-RF). Tracing the lines between the observed SPI-3 and the predicted one clearly showed an efficient performance of RF under the suggested SC3. It is interesting to note that the observational values were wider than the predicted ones. In this sense, the observed SPI-3 ranged between 3.43 and −4.19 in the SZO station, while the predicted one was [2.66, −3.29]. In the SZ station, the SPI-3 ranged from 3.09 to −3.4 and the predicted values were [2.609, −2.808] (Fig. 13). In the SZ station, the RF performance was good with a high NSE value and low RMSE (NSE = 0.88, r = 0.95, RMSE = 0.34). Similarly, in SZO the SC3-RF was good where NSE was 0.88, r was 0.95, and RMSE was 0.33 (Fig. 13).

4. Discussion

4.1. Future projections of climate and droughts indicators

Hydroclimatic shifts presented by drought events are a significant consequence of climatic change. Utilization of GCMs of CMIP6 provides a more precise assessment of global climatic scenarios in terms of temperature and precipitation change (Alaminie et al., 2021; Hersi et al., 2023; Zhang et al., 2022). Projected changes in the frequency and distribution pattern of precipitation events from high to low extremes relate to recurrent extreme events (Poschlod, 2022; Sauter et al., 2023; Zhao et al., 2023). Precipitation projections for the next century derived from CMIP6 global circulation models revealed an increase in rainfall in Asia, the Middle east and northeast Africa, and the continental land of north America and decrease in rainfall with high frequency forecasted droughts in the Mediterranean region, southwest Australia and Africa, and western coasts of south America (Cook et al., 2020). Overall, the precipitation pattern from SSP2-4.5 and SSP4-6.0 is projected to rise by the end of 2100 compared to historical (Fig. 5). It is expected that the annual maximum precipitation will experience a rise of over 100 mm/year. Additionally, the number of extreme rainy days is anticipated to increase by approximately 30 and 50 days during the mid and far future, respectively (Dhib and Halenka, 2022; Plavcová et al., 2023). However, the regional CORDEX simulations over central and northern Europe anticipated 20 % intense and extreme precipitation events in the winters. However, rainy days are expected to reduce in summers with short-term droughts occurrence. The European hydrological cycle is expected to undergo significant alterations, which may have substantial consequences for both environmental and anthropogenic systems (Rajczak and Schär, 2017). According to the simulations, there is a growing likelihood of summer droughts in central and southern Europe (Careto et al., 2022), while the frequency and intensity of heavy rainfall are

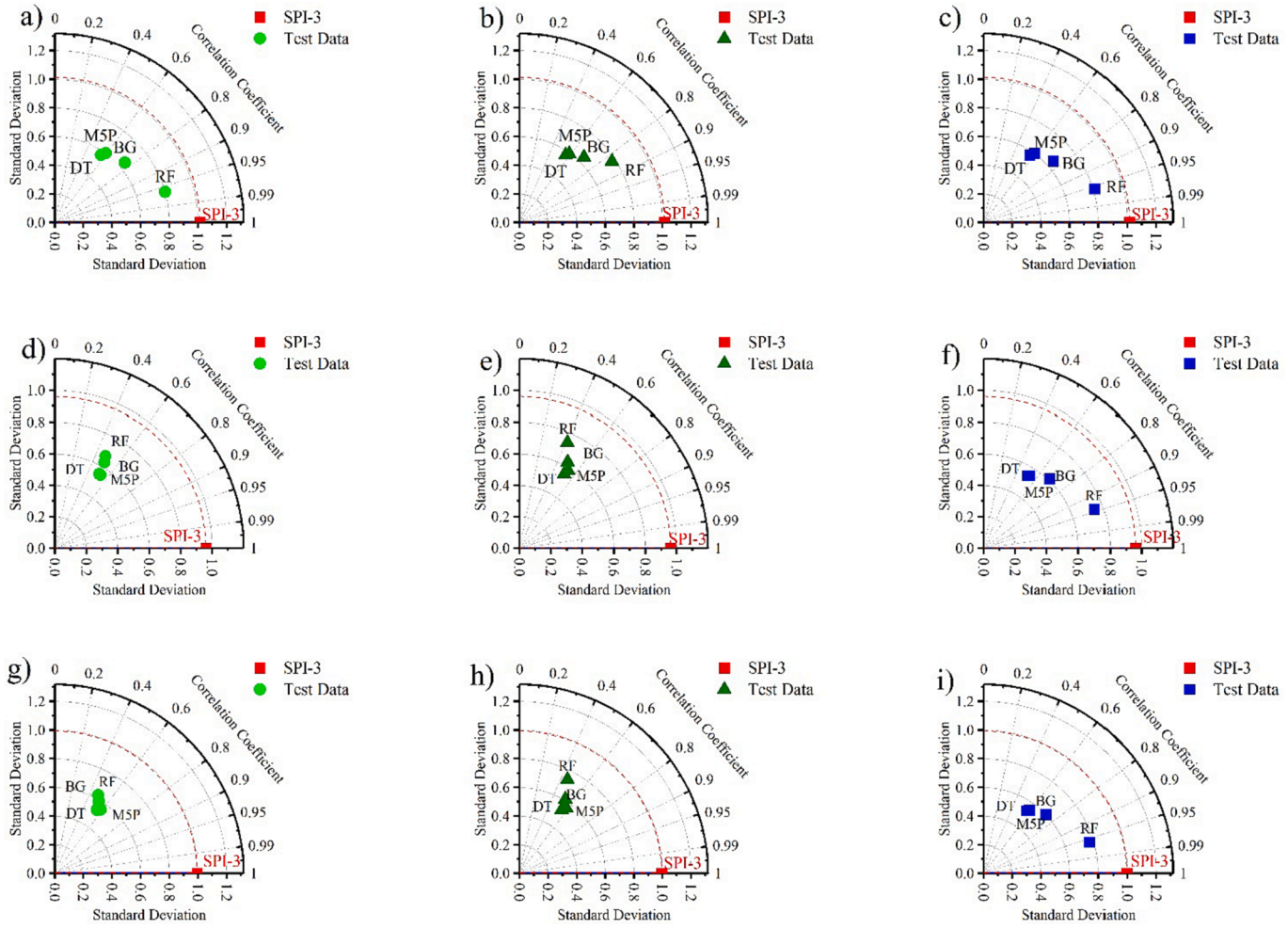

Fig. 10. Tylor diagram for Budapest (BD) station based on studied scenarios (a) algorithm performance in the training phase for SC1 ($R + T + T_{max} + T_{min}$), (b) algorithm performance in the cross-validation phase for SC1, (c) algorithm performance in the testing phase for SC1, (d) algorithm performance in the training phase for SC2 (R), (e) algorithm performance in cross-validation phase for SC2, (f) algorithm performance in the testing phase for SC2, (g) algorithm performance in the training phase for SC3 ($R + T$), h) algorithm performance in cross-validation phase for SC3, (i) algorithm performance in the testing phase for SC3. For all scenarios: the training phase is represented in a green circle, the cross-validation phase in an olive triangle, and the testing phase in a blue square. (For interpretation of the references to color in this figure legend, the reader is referred to the web version of this article.)

anticipated to increase across the entire continent (Rajczak and Schär, 2017). Regarding the SPI drought trend, our research findings suggested more droughts in the near future, but a substantial increase in the rain with less frequency of drought events in the mid and far future (2041–2100). It aligned with the findings of Wang et al. (2021), who also reported a decrease in drought in drought frequency and duration in the central north of Europe (NEU) evaluated from 11 GCMs of CMIP6 by the end of the 21st century. Another study by Zhao et al. (2023) reported a moderate level of short-term drought forecast in northern central Europe from CanESM2 and CESM1. In addition, the projected temperature from three GCMs showed a rising trend of temperature in both scenarios. However, SSP460 predicts higher temperatures and unprecedented rainfalls due to limited mitigation efforts. (Fig. 6 and Table A2) (Mondal et al., 2021).

4.2. Atmospheric factors for present and future drought occurrence

In the past decades, meteorological drought events were more frequent over central and northern Europe (Spinoni et al., 2019) which are attributed to several atmospheric phenomenon. Hungary, as a regional representative of central Europe in our research, experienced short-term drought events in the years 1925, 1947,1949, 1950, 2000, and 2003 across the selected stations in the past (Fig. 7). Based on SSPs scenarios of rainfall projections, extreme droughts events are expected to occur in years 2028, 2031, 2032, 2034, 2040 in NF and 2096–99 in FF. In the past few decades, the European region has begun warming in an unprecedented way (Hernández-Morcillo et al., 2018). This warming combined with an increase in the frequency and severity of drought events across Europe (Hanel et al., 2018; Van Lanen et al., 2016). Throughout the last two decades, Central Europe has been plagued by long-lasting compound extreme events i.e., drought and heat waves (Hari et al., 2020a). For example, in recent years 2018–19, the region experienced heat waves and severe droughts due to abnormal atmospheric conditions, like anticyclonic circulation patterns and higher geopotential height anomalies. These are linked to longer drying trends with low precipitation, high temperatures, reduced soil moisture, and increased evapotranspiration rates. Consequently, the river flow in central Europe dropped to record lows (Ionita and Nagavciuc, 2020). These prolonged dry spells were accompanied by an increase in the anticyclonic weather patterns, as well as a persistent high-pressure system (Fleig et al., 2011), that is centered over the North Sea and Germany and is bordered by low-pressure systems over the central North Atlantic region and western Siberia (Ionita et al., 2020). Due to these high-pressure centers, warm and dry air is advected from the eastern part of Europe, resulting in increased solar radiation, which decreased precipitation and soil moisture (Buehler et al., 2011). In three historical

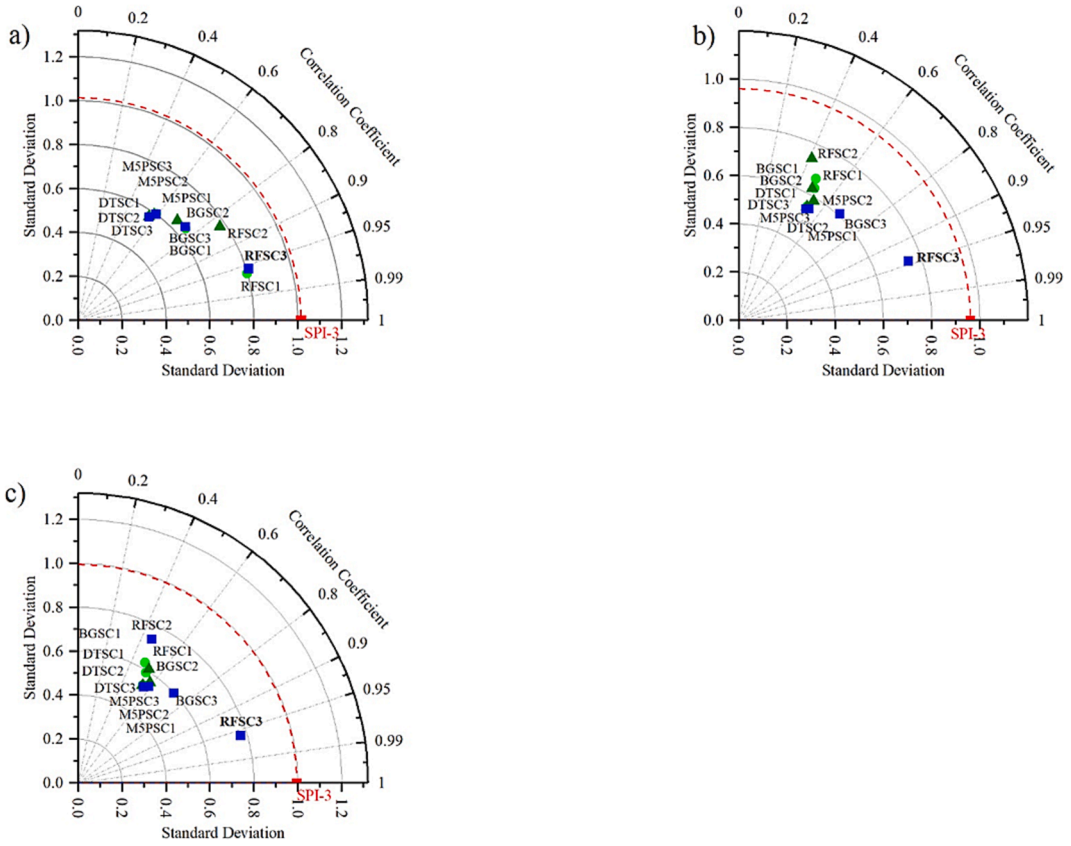

Fig. 11. Algorithm performance based on Tylor diagram for Budapest (BD) in (a) training phase for SC1 ($R + T + T_{max} + T_{min}$)/green circle, SC2 ($R$)/olive triangle and SC3 ($R + T$)/blue square, (b) cross-validation phase for SC1 ($R + T + T_{max} + T_{min}$)/green circle, SC2 ($R$)/olive triangle and SC3 ($R + T$)/blue square, and c) testing phase for SC1 ($R + T + T_{max} + T_{min}$)/green circle, SC2 ($R$)/olive triangle, and SC3 ($R + T$)/blue square. (For interpretation of the references to color in this figure legend, the reader is referred to the web version of this article.)

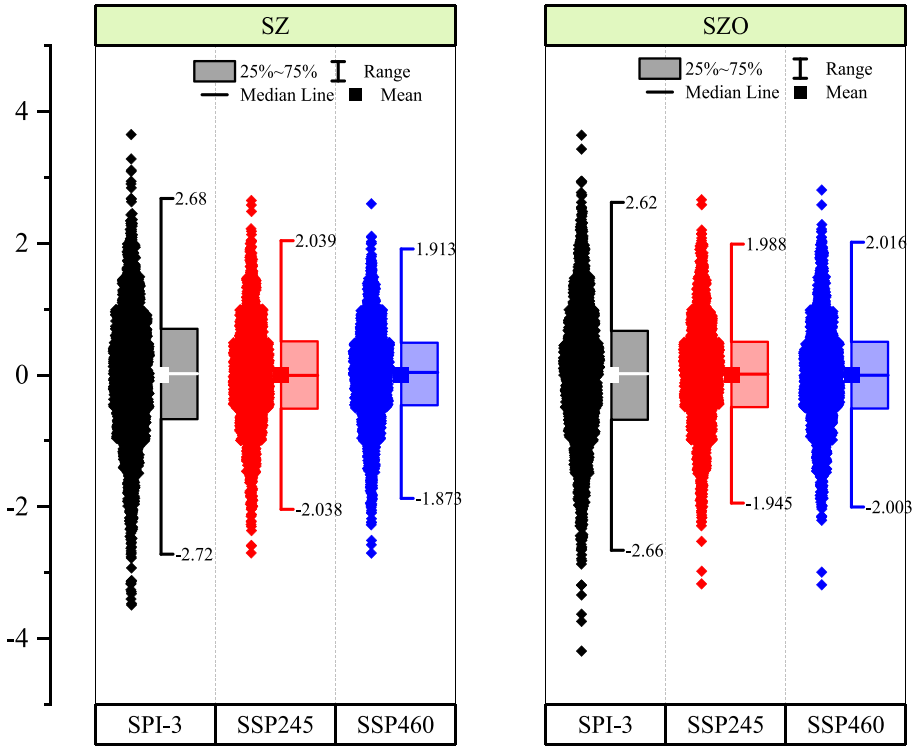

Fig. 12. Boxplot for observed and predicted SPI-3 values-based RF-SC3 in Szeged (SZ) and Szombathely (SZO) stations.

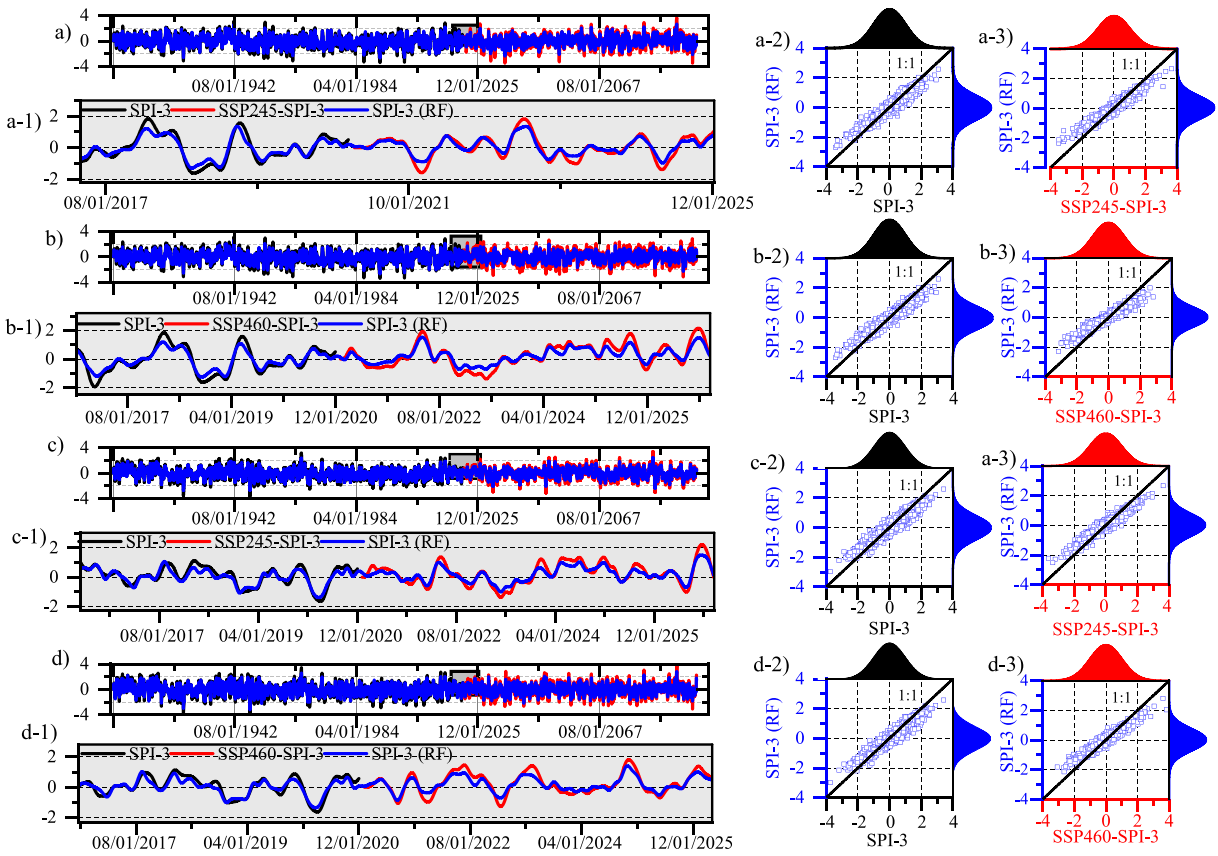

Fig. 13. Calculated (HS + SSPs) and predicted (RF) SPI-3 values in Szeged (SZ) and Szombathely (SZO) stations between 1901 and 2100: (a) observed (HS + SSP245) vs. predicted (RF) SPI-3 in SZ (1901–20100); (a-1) zoom in (2017–2025), (a-2) scatter plot SPI-3 (HS) vs SPI-3 (RF), (a-3) scatter plot SPI-3 (SSP245) vs SPI-3 (RF); (b) observed (HS + SSP460) vs. predicted (RF) SPI-3 in SZ (1901–20100); (b-1) zoom in (2017–2025), (b-2) scatter plot SPI-3 (HS) vs SPI-3 (RF), a-3) scatter plot SPI-3 (SSP460) vs SPI-3 (RF); (c) observed (HS + SSP245) vs. predicted (RF) SPI-3 in SZO (1901–20100); (c-1) zoom in (2017–2025), (c-2) scatter plot SPI-3 (HS) vs SPI-3 (RF), (c-3) scatter plot SPI-3 (SSP245) vs SPI-3 (RF); (d) observed (HS + SSP460) vs. predicted (RF) SPI-3 in SZO (1901–20100); (d-1) zoom in (2017–2025), (d-2) scatter plot SPI-3 (HS) vs SPI-3 (RF), (d-3) scatter plot SPI-3 (SSP460) vs SPI-3 (RF).

compound extreme events years 1994, 2006, and 2015,(Ionita et al., 2017; Lhotka et al., 2018; Tomczyk and Bednorz, 2019) central Europe experienced similar reasons for climatological changes. These conditions combined with other abnormal disturbances in primary jet streams caused due to high-pressure spots such as over the North Sea, potentially increased the severity and frequency of major last drought events across north Europe and central Europe (Zhang et al., 2020). Based on the climatic pattern and atmospheric circulations of the region, future climatic projections under high-emission scenarios indicates a high probaility of droughts in far future but less probability of drought occurrence in low emission scenarios especially in RCP 2.6 and 4.5 (Hari et al., 2020b).

4.3. Applicability of performance of machine learning (ML) techniques for drought forecasting

In the recent decades of an increasing trend of climatic extremes, high computational speed, and the ability to handle big data complexities have made ML a preferable choice for disaster prediction, forecasting, and management (Pourghasemi et al., 2020; Prodhan et al., 2022). Drought prediction using ML methods like RF, SVM, XGBoost, and Neural networks provides more accurate results as compared to traditional statistical and probabilistic approaches. However, the performance accuracy of each ML method varies in different scenarios at different scales (Aghelpour et al., 2020; Prodhan et al., 2022; Wahla et al., 2024; Zhang et al., 2019).

In the context of ML applications, our study implemented four algorithms (BG, RF, M5P & DT) to predict short-term droughts using SPI-3 in three different climatic scenarios. Many drought prediction studies utilized ML algorithms using a random selection approach for model training, testing, and validation (Khan et al., 2020; Mohammed et al., 2022; Rahmati et al., 2020). Currently, model implementation at BD station i.e., taken as a standard to explore the best ML algorithm and scenario also uses a random division approach. The major finding revealed RF outperformed other ML algorithms for SC3 in the testing and validation stage while DT proved to be less accurate for SPI prediction in all scenarios. (Figs. 8–11). The reason for low performance of DT is linked to its binary condition rule which makes it less accurate to capture the complex relationships. Moreover, the redundant rules of DTs increase the risk of error with underfitting (Huang et al., 2022). In contrast, RF provides advantageous results in many prediction studies (Park et al., 2016; Park et al., 2018) because it uses several decision trees along with a bagging approach which prevents the model from overfitting. In short, it provides a better unbiased generalization of predicted results over the region (Kuswanto and Naufal, 2019; Lotfirad et al., 2021). However, our findings of SC1 revealed a high performance of RF with r = 0.96 in the training stage and a lower performance in the testing stage with r = 0.48 suggesting an overfitting in the training stage but less effective to learn on unseen data in the testing stage. This presents a nuanced model behavior that can be improved by adding regularization techniques (Montesinos López et al., 2022). Furthermore, in SC2 and SC3 RF performance proved to be more satisfactory compared to other algorithms making it superior to apply for future SPI predicitons in SSP2-4.5 and SSP4-6.0. Overall, the current high performance of RF is aligned with the findings of Elbeltagi et al., (2023a) with a high predictive performance of SPI drought. This is attributed to its ability to

handle large datasets and its excellent interpretability, especially when dealing with many characteristics (Rahmati et al., 2020). It generates a tree-based regression function, it eliminates the need for scaling between different features, which is a considerable advantage in cases with multiple features (Liaw and Wiener, 2002).

Besides this, 4 climatic predictors i.e., (T, T_{max}, T_{min}, R) used for developed scenarios (SC1, SC2 and SC3) also provided significant findings in our study. Rainfall and temperature ($R + T$) i.e., SC3 proved to be the best scenario for short-term drought prediction (Figs. 8–10). Multiple climatic variables are used for drought predictions. For example, Deo et al. (2018) used 12 predictors including rainfall, minimum, maximum, and mean temperature, evapotranspiration, and oscillation-based indices for short-term SPEI drought predictions using ML algorithms. A similar study conducted by Khan et al. (2020) used 6 climatic predictors including temperature, relative humidity, wind and Geopotential height, and sea level pressure for agriculture drought predictions. ML-based prediction from SC3 over a large dataset in our study proved its applicability for other drought indices and accurate future projections of drought events. It is anticipated that the severity of droughts will increase in the future under high greenhouse gas emission scenarios, thus disrupting the hydrological ecosystem. Therefore, our study holds significant implications for the optimization of water resource management in agricultural ecosystems in the near to far future. Furthermore, the accurate predictions from the Random Forest algorithm on a substantial dataset spanning 100–200 years demonstrates the susceptibility of central Europe to recurrent and severe drought events, thereby offering its applicability in other European regions as well.

5. Research limitations

Overall, our study provided meaningful findings in terms of identification and forecasting of short-term meteorological drought i.e., SPI-3 based on historical and projected long-term climatic time series of two centuries (1901–2100) employing various ML methods. SPI-3 is a WMO-recommended and widely used drought index to monitor the short-term soil moisture deficit, but it is derived from the sole utilization of rainfall data only which limits its capability to examine the droughts on a wider scale. Predicting or forecasting the short-term SPI-3 drought from other climatic variables proved to be a good approach but due to the limitations in data availability only three climatic indicators namely, minimum, maximum, and mean temperature are being used currently along with rainfall for predicting SPI-3. However, the prediction accuracy can be further improved by incorporating other climatic factors like wind speed, air pressure, relative humidity, vapor pressure, evapotranspiration, etc. (Deo et al., 2018; Khan et al., 2020). Our research is currently based on the limited ensemble of GCMs and does not have more variations by adding more GCMs and RCMs. Hence, the inclusion of multiple GCMs in more SSPs followed by standard validation procedures would increase the reliability of forecasting future drought events. In terms of ML applications, we examined the capability of most tree-based algorithms which we intend to extend to other methods including neural networks (NN), support vector regressors (SVR), boosting, Gaussian process regression (GPR) (Iranshahi et al., 2023; Maca and Pech, 2016; Yaseen et al., 2021). We divided the time series into three datasets for training, testing, and cross-validation. This approach helped to prevent overfitting and ensured reliable machine learning performance. Hyperparameter tuning can further improve accuracy with complex algorithms (Prodhan et al., 2022). Moreover, in the future, evaluating the model's significance through relative importance analysis can provide more insight into the factors associated with drought occurrence.

6. Conclusion

Drought is a multiscalar and complex climatic extreme with long-lasting impacts on the natural ecosystem. Hence, accurate drought prediction over a longer time is crucial for developing mitigation and adaptation strategies. In this context, our study focussed on short-term drought prediction using SPI-3 at three sampled stations in central Europe over a longer time (i.e., historical (1901–2020) and future (2021–2100)) using four ML algorithms.

The major output of this research is summarized as follows.

1. The mean historical (1901–2020) rain is observed to be between 535 and 632 mm which is projected (2021–2100) to exceed 600–700 mm in the NF and MF.
2. The average temperature for the HS data ranged from 9.6 °C in SZO to 11.39 °C in BD. Under different climate scenarios, this is projected to be increased to reach 17 °C and 19 °C.
3. Drought events increased after 1970. Further, projected SPI-3 revealed an increasing trend of short-term agricultural drought in NF (2021–2040). However, more frequent droughts are projected under ssp460.
4. Among a combination of different climatic scenarios to predict SPI-3 (i.e., SC1($R + T + T_{max} + T_{min}$), SC2 ($R$), and SC3 ($R + T$)), the SC3 is found to be best for SPI-3 prediction.
5. Although 4 ML (BG, DT, M5P, RF) algorithms varied in their ability for SPI-3 drought prediction. However, RF outperformed other algorithms for accurate prediction in cross-validation and testing stages at standard BD stations. However, the RF was able to predict the SPI-3 values more accurately than other algorithms.
6. The SC3 ($R + T$) with RF implementation at the remaining two stations revealed high accuracy.

In conclusion, our study validates the performance of the RF algorithm for short-term drought monitoring with total monthly rainfall and mean monthly temperature ($R + T$) as a major determining factor of meteorological drought over extended periods.

CRediT authorship contribution statement

Safwan Mohammed: Data curation, Visualization, Writing – original draft, Methodology, Formal analysis. **Sana Arshad:** Methodology, Writing – original draft. **Firas Alsilibe:** Writing – review & editing. **Muhammad Farhan Ul Moazzam:** Writing – review & editing. **Bashar Bashir:** Writing – review & editing. **Foyez Ahmed Prodhan:** Formal analysis. **Abdullah Alsalman:** Writing – review & editing. **Attila Vad:** Writing – review & editing. **Tamás Ratonyi:** Writing – review & editing. **Endre Harsányi:** Supervision, Writing – review & editing.

Declaration of competing interest

The authors declare that they have no known competing financial interests or personal relationships that could have appeared to influence the work reported in this paper.

Data availability

Data will be made available on request.

Acknowledgement

The authors wish to express their gratitude to the anonymous reviewers and editors for their insightful comments and advice, which significantly improved the quality of this work. Furthermore, this work was made possible with the support of the University of Debrecen's Publication Science Support Program.

Funding

This research was supported by the Researchers Supporting Project, Grant number (RSP2024R296), King Saud University, Riyadh, Saudi Arabia. Also, Project no. TKP2021-NKTA-32 has been implemented with

support from Hungary's National Research, Development, and Innovation Fund, financed under the TKP2021-NKTA funding scheme.

Appendix

Table A1
Descriptive statistics of the studied climate stations (SZO, SZ, BD) for the period 1901–2020 in Hungary.

Station*	Statistic	Min.	Max.	Range	Median	Mean	SD.	SK.	KR.
SZO	R	0.3	224.4	224.1	45.3	52.7	36.1	1.1	1.1
	T	−10.3	24.4	34.7	9.9	9.6	7.7	−0.1	−1.2
	T_{max}	−2.4	29.7	32.1	16.1	15.5	7.2	−0.2	−1.1
	T_{min}	−20.9	18.8	39.7	4.0	3.6	8.5	−0.3	−1.0
SZ	R	0.0	199.0	199.0	37.7	44.6	31.0	1.2	1.9
	T	−9.5	25.7	35.2	11.4	11.0	8.3	−0.2	−1.2
	T_{max}	−2.1	31.8	33.9	17.8	17.3	7.9	−0.2	−1.1
	T_{min}	−21.9	20.9	42.8	4.9	4.4	9.2	−0.3	−0.9
BD	R	0.0	263.1	263.1	42.8	48.5	33.4	1.3	2.9
	T	−8.7	26.6	35.3	11.5	11.3	8.0	−0.1	−1.2
	T_{max}	−2.9	33.1	36.0	18.1	17.4	7.7	−0.2	−1.2
	T_{min}	−20.6	21.7	42.3	5.5	5.1	8.5	−0.2	−1.0

* $n = 1440$ months, min: minimum, max: maximum, SD: standard deviation (n), SK: Skewness (Pearson), KR: Kurtosis (Pearson).

Table A2
Mann-Kendall trend and Sen's slope analysis of historical (1901–2020) and projected in near future (NF) (2021–2040), middle future (MF) (2041–2070), and far future (FF) (2071–2100) climatic variables (R, Tmax, and Tmin) under SSP2 and SSP4 scenarios at three stations (BD, SZ, and SZO) in Hungary, Cental Europe.

	SSP245					SSP460			
Station	var	Tau	P-value	Sen'sslope	BR	Tau	P-value	Sen'sslope	BR
BD	**Rain(His)**	**−0.19*****	**0.001**	−1.01	1970	**−0.19*****	**0.001**	−1.01	1970
	Rain (NF)	−0.13	0.4	−1.81		−0.11	0.4	−1.29	
	Rain (MF)	0.23	0.07	2.60		0.14	0.2	2.2	
	Rain (FF)	0.13	0.31	1.8		0.11	0.37	1.22	
	Tmax(His)	**0.27*****	**>0.001**	**0.01**	1986	**0.27*****	**>0.001**	**0.01**	1986
	Tmax (NF)	0.23	0.16	0.02		**0.63*****	**>0.001**	0.08	
	Tmax (MF)	0.07	0.56	0.007		**0.35****	**0.006**	0.02	
	Tmax (FF)	0.22	0.08	0.02		0.10	0.41	0.007	
	Tmin(His)	**0.23*****	**>0.001**	**0.03**	1969	**0.23*****	**>0.001**	**0.03**	1969
	Tmin (NF)	0.27	0.09	0.02		0.55***	>0.001	0.05	
	Tmin (MF)	0.31**	0.01	0.01		0.45***	>0.001	0.02	
	Tmin (FF)	0.18	0.15	0.01		0.23	0.07	0.01	
SZ	**Rain(his)**	−0.10	0.07	−0.50	1944	−0.10	0.07	−0.50	1944
	Rain (NF)	−0.13	0.4	−1.7		−0.12	0.45	−1.73	
	Rain (MF)	0.18	0.16	1.35		0.13	0.3	1.91	
	Rain (FF)	0.02	0.85	0.27		−0.04	0.72	−0.50	
	Tmax(His)	**−0.04**	**0.50**	**−0.003**	1961	**−0.04**	**0.50**	**−0.003**	1961
	Tmax (NF)	0.29	0.07	0.03		**0.62*****	**>0.001**	0.08	
	Tmax (MF)	0.12	0.3	0.01		**0.30****	**0.01**	0.02	
	Tmax (FF)	0.28	0.02	0.02		0.13	0.30	0.009	
	Tmin(His)	**0.13***	**0.03**	**0.02**	1969	**0.13**	**0.03**	**0.02**	1969
	Tmin (NF)	0.30	0.06	0.02		**0.654*****	**>0.001**	0.05	
	Tmin (MF)	**0.29***	**0.02**	0.02		**0.48*****	**>0.001**	0.02	
	Tmin (FF)	**0.30***	**0.02**	0.02		0.19	0.14	0.009	
SZO	**Rain(His)**	**−0.15****	**0.01**	−0.75	1966	**−0.15****	**0.01**	−0.75	1966
	Rain (NF)	−0.2	0.2	−2.1		−0.26	0.11	−4.32	
	Rain (MF)	0.21	0.09	1.2		0.05	0.6	1.20	
	Rain (FF)	0.10	0.43	1.37		0.006	0.9	0.18	
	Tmax(His)	**0.18****	**0.002**	**0.01**	**1982**	**0.18****	**0.002**	**0.01**	**1982**
	Tmax (NF)	0.21	0.20	0.02		**0.61*****	**>0.001**	0.08	
	Tmax (MF)	0.14	0.2	0.009		**0.31****	**0.01**	0.02	
	Tmax (FF)	**0.25***	**0.04**	0.02		0.11	0.37	0.008	
	Tmin(His)	**0.18****	**0.002**	**0.02**	**1971**	**0.18****	**0.002**	**0.02**	**1971**
	Tmin (NF)	**0.31***	**0.05**	0.02		**0.56*****	**>0.001**	0.06	
	Tmin (MF)	**0.29***	**0.02**	0.01		**0.41*****	**0.001**	0.02	
	Tmin (FF)	**0.34****	**0.008**	0.02		**0.25***	**0.04**	0.01	

Table A3
Statistical results of training (TR), cross-validation (CrV), and testing (TS) for the BD station.

TR	BGSC1	DTSC1	M5PSC1	RFSC1	BGSC2	DTSC2	M5PSC2	RFSC2	BGSC3	DTSC3	M5PSC3	RFSC3
NSE	0.56	0.31	0.32	0.89	0.49	0.31	0.34	0.69	0.52	0.31	0.34	0.89
RMSE	0.67	0.87	0.81	0.32	0.72	0.83	0.88	0.56	0.67	0.83	0.81	0.33
MAEr	0.53	0.67	0.65	0.25	0.57	0.67	0.66	0.43	0.54	0.67	0.65	0.26
r	0.76	0.54	0.57	0.96	0.7	0.74	0.76	0.83	0.75	0.56	0.59	0.95
DAg	0.81	0.65	0.68	0.96	0.77	0.65	0.67	0.89	0.811	0.65	0.68	0.96
CrV	**BGSC1**	**DTSC1**	**M5PSC1**	**RFSC1**	**BGSC2**	**DTSC2**	**M5PSC2**	**RFSC2**	**BGSC3**	**DTSC3**	**M5PSC3**	**RFSC3**
NSE	0.21	0.25	0.26	0.16	0.19	0.23	0.26	0.018	0.46	0.25	0.27	0.86
RMSE	0.82	0.82	0.82	0.876	0.85	0.82	0.81	0.95	0.7	0.82	0.81	0.35
MAEr	0.68	0.66	0.65	0.69	0.68	0.66	0.65	0.77	0.55	0.66	0.65	0.276
r	0.49	0.51	0.52	0.48	0.48	0.51	0.53	0.41	0.68	0.51	0.53	0.94
DAg	0.62	0.62	0.62	0.61	0.61	0.61	0.63	0.56	0.76	0.6	0.62	0.95
TS	**BGSC1**	**DTSC1**	**M5PSC1**	**RFSC1**	**BGSC2**	**DTSC2**	**M5PSC2**	**RFSC2**	**BGSC3**	**DTSC3**	**M5PSC3**	**RFSC3**
NSE	0.26	0.29	0.33	0.21	0.26	0.26	0.33	0.21	0.51	0.3	0.33	0.88
RMSE	0.85	0.83	0.8	0.88	0.85	0.83	0.81	0.91	0.69	0.82	0.8	0.33
MAEr	0.67	0.67	0.64	0.69	0.66	0.67	0.65	0.73	0.55	0.67	0.64	0.27
r	0.52	0.55	0.58	0.48	0.52	0.55	0.58	0.45	0.72	0.56	0.58	0.96
DAg	0.68	0.62	0.65	0.6	0.63	0.62	0.66	0.6	0.78	0.63	0.66	0.96

References

Acharki, S., Singh, S.K., do Couto, E.V., Arjdal, Y., Elbeltagi, A., 2023. Spatio-temporal distribution and prediction of agricultural and meteorological drought in a Mediterranean coastal watershed via GIS and machine learning. Phys. Chem. Earth, Parts A/B/C 131, 103425. https://doi.org/10.1016/j.pce.2023.103425.

Achite, M., Jehanzaib, M., Elshaboury, N., Kim, T.-W., 2022. Evaluation of machine learning techniques for hydrological drought modeling: a case study of the Wadi Ouahrane Basin in Algeria. Water 14 (3), 431.

Achite, M., Elshaboury, N., Jehanzaib, M., Vishwakarma, D., Pham, Q., Anh, D., Abdelkader, E., Elbeltagi, A., 2023. Performance of machine learning techniques for meteorological drought forecasting in the Wadi Mina Basin, Algeria. Water 15 (4), 765.

Adeyeri, O.E., Zhou, W., Laux, P., Ndehedehe, C.E., Wang, X., Usman, M., Akinsanola, A. A., 2023. Multivariate drought monitoring, propagation, and projection using bias-corrected general circulation models. earth's. Future 11 (4). https://doi.org/10.1029/2022EF003303.

Adnan, R.M., Dai, H.-L., Kuriqi, A., Kisi, O., Zounemat-Kermani, M., 2023. Improving drought modeling based on new heuristic machine learning methods. Ain Shams Eng. J. 14 (10), 102168 https://doi.org/10.1016/j.asej.2023.102168.

Agana, N.A., Homaifar, A., 2017. A deep learning based approach for long-term drought prediction. SoutheastCon 2017, 1–8. https://doi.org/10.1109/SECON.2017.7925314.

Aghelpour, P., Mohammadi, B., Biazar, S.M., Kisi, O., Sourmirinezhad, Z., 2020. A theoretical approach for forecasting different types of drought simultaneously, using entropy theory and machine-learning methods. ISPRS Int. J. Geo Inf. 9 (12), 701. https://doi.org/10.3390/ijgi9120701.

Alaminie, A.A., Tilahun, S.A., Legesse, S.A., Zimale, F.A., Tarkegn, G.B., Jury, M.R., 2021. Evaluation of past and future climate trends under CMIP6 scenarios for the UBNB (Abay), Ethiopia. Water 13 (15), 2110.

Alsafadi, K., Bi, S., Abdo, H.G., Almohamad, H., Alatrach, B., Srivastava, A.K., Al-Mutiry, M., Bal, S.K., Chandran, M.A.S., Mohammed, S., 2023. Modeling the impacts of projected climate change on wheat crop suitability in semi-arid regions using the AHP-based weighted climatic suitability index and CMIP6. Geosci. Lett. 10 (1) https://doi.org/10.1186/s40562-023-00273-y.

Arabameri, A., Chandra Pal, S., Santosh, M., Chakrabortty, R., Roy, P., Moayedi, H., 2022. Drought risk assessment: integrating meteorological, hydrological, agricultural and socio-economic factors using ensemble models and geospatial techniques. Geocarto Int. 37 (21), 6087–6115. https://doi.org/10.1080/10106049.2021.1926558.

Arshad, S., Kazmi, J.H., Javed, M.G., Mohammed, S., 2023a. Applicability of machine learning techniques in predicting wheat yield based on remote sensing and climate data in Pakistan, South Asia. Eur. J. Agron. 147, 126837. https://doi.org/10.1016/j.eja.2023.126837.

Arshad, S., Kazmi, J.H., Prodhan, F.A., Mohammed, S., 2023b. Exploring dynamic response of agrometeorological droughts towards winter wheat yield loss risk using machine learning approach at a regional scale in Pakistan. Field Crop Res 302, 109057. https://doi.org/10.1016/j.fcr.2023.109057.

Bazrafshan, J., 2017. Effect of air temperature on historical trend of long-term droughts in different climates of Iran. Water Resour. Manag. 31 (14), 4683–4698. https://doi.org/10.1007/s11269-017-1773-8.

Belayneh, A., Adamowski, J., Khalil, B., 2016a. Short-term SPI drought forecasting in the Awash River basin in Ethiopia using wavelet transforms and machine learning methods. Sustain. Water Resour. Manage. 2 (1), 87–101. https://doi.org/10.1007/s40899-015-0040-5.

Belayneh, A., Adamowski, J., Khalil, B., Quilty, J., 2016b. Coupling machine learning methods with wavelet transforms and the bootstrap and boosting ensemble approaches for drought prediction. Atmos. Res. 172–173, 37–47. https://doi.org/10.1016/j.atmosres.2015.12.017.

Blauhut, V., et al., 2022. Lessons from the 2018–2019 European droughts: a collective need for unifying drought risk management. Nat. Hazards Earth Syst. Sci. 22 (6), 2201–2217. https://doi.org/10.5194/nhess-2021-276.

Breiman, L., 1996. Bagging predictors. Mach. Learn. 24 (2), 123–140. https://doi.org/10.1007/BF00058655.

Breiman, L., 2001. Random forests. Mach. Learn. 45 (1), 5–32. https://doi.org/10.1023/A:1010933404324.

Buehler, T., Raible, C.C., Stocker, T.F., 2011. The relationship of winter season North Atlantic blocking frequencies to extreme cold or dry spells in the ERA-40. Tellus A 63 (2), 212–222. https://doi.org/10.1111/j.1600-0870.2010.00492.x.

Buzási, A., 2021. Climate vulnerability and adaptation challenges in Szekszárd wine region. Hungary. Climate 9 (2), 25. https://doi.org/10.3390/cli9020025.

Buzási, A., Pálvölgyi, T., Esses, D., 2021. Drought-related vulnerability and its policy implications in Hungary. Mitig. Adapt. Strat. Glob. Chang. 26 (3), 11. https://doi.org/10.1007/s11027-021-09943-8.

Careto, J.A., Soares, P.M., Cardoso, R.M., Russo, A., Lima, D.C., 2022. A new ensemble-based SPI and SPEI index to depict droughts projections for the Iberia Peninsula with the EURO-CORDEX, EGU General Assembly Conference Abstracts, pp. EGU22-12405. DOI: 10.5194/egusphere-egu22-12405.

Ceglar, A., Croitoru, A.-E., Cuxart, J., Djurdjevic, V., Güttler, I., Ivančan-Picek, B., Jug, D., Lakatos, M., Weidinger, T., 2018. PannEx: The Pannonian Basin experiment. Clim. Serv. 11, 78–85. https://doi.org/10.1016/j.cliser.2018.05.002.

Chen, Y.S., 2016. An empirical study of a hybrid imbalanced-class DT-RST classification procedure to elucidate therapeutic effects in uremia patients. Med. Biol. Eng. Comput. 54 (6), 983–1001. https://doi.org/10.1007/s11517-016-1482-0.

Cook, B.I., Mankin, J.S., Marvel, K., Williams, A.P., Smerdon, J.E., Anchukaitis, K.J., 2020. Twenty-first century drought projections in the CMIP6 forcing scenarios. Earth's Future 8 (6). https://doi.org/10.1029/2019EF001461.

Csete, M.S., Barna, O., 2021. Assessment of regional climate innovation potential in Hungary. Int. J. Global Warm. 25 (3–4), 378–389. https://doi.org/10.1504/IJGW.2021.119007.

Dayal, K., Deo, R., Apan, A.A., 2017. Drought modelling based on artificial intelligence and neural network algorithms: A case study in Queensland, Australia. In: Leal Filho, W. (Ed.), Climate Change Adaptation in Pacific Countries: Fostering Resilience and Improving the Quality of Life. Springer International Publishing, Cham, pp. 177–198. https://doi.org/10.1007/978-3-319-50094-2_11.

Deo, R.C., Tiwari, M.K., Adamowski, J.F., Quilty, J.M., 2017. Forecasting effective drought index using a wavelet extreme learning machine (W-ELM) model. Stoch. Env. Res. Risk A 31 (5), 1211–1240. https://doi.org/10.1007/s00477-016-1265-z.

Deo, R.C., Salcedo-Sanz, S., Carro-Calvo, L., Saavedra-Moreno, B., 2018. Chapter 10 – Drought prediction with standardized precipitation and evapotranspiration index and support vector regression models. In: Samui, P., Kim, D., Ghosh, C. (Eds.), Integrating Disaster Science and Management. Elsevier, pp. 151–174. https://doi.org/10.1016/B978-0-12-812056-9.00010-5.

Dhib, S., Halenka, T., 2022. Projected Climate Change Indices over Central Europe Using Dynamically Downscaled CMIP6 Models, EGU General Assembly Conference Abstracts, pp. EGU22-11053. https://doi.org/10.5194/egusphere-egu22-11053.

Dikshit, A., Pradhan, B., Santosh, M., 2022. Artificial neural networks in drought prediction in the 21st century–A scientometric analysis. Appl. Soft Comput. 114, 108080 https://doi.org/10.1016/j.asoc.2021.108080.
Djerbouai, S., Souag-Gamane, D., 2016. Drought forecasting using neural networks, wavelet neural networks, and stochastic models: case of the Algerois Basin in North Algeria. Water Resour. Manag. 30 (7), 2445–2464. https://doi.org/10.1007/s11269-016-1298-6.
Elbeltagi, A., Pande, C.B., Kumar, M., Tolche, A.D., Singh, S.K., Kumar, A., Vishwakarma, D.K., 2023a. Prediction of meteorological drought and standardized precipitation index based on the random forest (RF), random tree (RT), and Gaussian process regression (GPR) models. Environ. Sci. Pollut. Res. Int. 30 (15), 43183–43202.
Elbeltagi, A., Srivastava, A., Deng, J., Li, Z., Raza, A., Khadke, L., Yu, Z., El-Rawy, M., 2023b. Forecasting vapor pressure deficit for agricultural water management using machine learning in semi-arid environments. Agric. Water Manag. 283, 108302. https://doi.org/10.1016/j.agwat.2023.108302.
Fahimi, F., Yaseen, Z.M., El-shafie, A., 2017. Application of soft computing based hybrid models in hydrological variables modeling: a comprehensive review. Theor. Appl. Climatol. 128 (3), 875–903. https://doi.org/10.1007/s00704-016-1735-8.
Felsche, E., Ludwig, R., 2021. Applying machine learning for drought prediction in a perfect model framework using data from a large ensemble of climate simulations. Nat. Hazards Earth Syst. Sci. 21 (12), 3679–3691. https://doi.org/10.5194/nhess-21-3679-2021.
Feng, P., Wang, B., Liu, D.L., Yu, Q., 2019. Machine learning-based integration of remotely-sensed drought factors can improve the estimation of agricultural drought in South-Eastern Australia. Agric. Syst. 173, 303–316. https://doi.org/10.1016/j.agsy.2019.03.015.
Fleig, A.K., Tallaksen, L.M., Hisdal, H., Hannah, D.M., 2011. Regional hydrological drought in North-Western Europe: linking a new regional drought area index with weather types. Hydrol. Process. 25 (7), 1163–1179. https://doi.org/10.1002/hyp.7644.
Forzieri, G., Feyen, L., Rojas, R., Flörke, M., Wimmer, F., Bianchi, A., 2014. Ensemble projections of future streamflow droughts in Europe. Hydrol. Earth Syst. Sci. 18 (1), 85–108.
Gálos, B., Lorenz, P., Jacob, D., 2007. Will dry events occur more often in Hungary in the future? Environ. Res. Lett. 2 (3), 034006 https://doi.org/10.1088/1748-9326/2/3/034006.
Ganguli, P., Reddy, M.J., 2014. Ensemble prediction of regional droughts using climate inputs and the SVM–COPULA approach. Hydrol. Process. 28 (19), 4989–5009. https://doi.org/10.1002/hyp.9966.
Gao, W., Alsarraf, J., Moayedi, H., Shahsavar, A., Nguyen, H., 2019. Comprehensive preference learning and feature validity for designing energy-efficient residential buildings using machine learning paradigms. Appl. Soft Comput. 84, 105748 https://doi.org/10.1016/j.asoc.2019.105748.
Granata, F., Di Nunno, F., 2021. Artificial intelligence models for prediction of the tide level in Venice. Stoch. Env. Res. Risk A 35 (12), 2537–2548. https://doi.org/10.1007/s00477-021-02018-9.
Guttman, N.B., 1999. Accepting the standardized precipitation index: A calculation algorithm. JAWRA J. Am. Water Resour. Assoc. 35 (2), 311–322. https://doi.org/10.1111/j.1752-1688.1999.tb03592.x.
Hanel, M., Rakovec, O., Markonis, Y., Máca, P., Samaniego, L., Kyselý, J., Kumar, R., 2018. Revisiting the recent European droughts from a long-term perspective. Sci. Rep. 8 (1) https://doi.org/10.1038/s41598-018-27464-4.
Hänsel, S., Ustrnul, Z., Łupikasza, E., Skalak, P., 2019. Assessing seasonal drought variations and trends over Central Europe. Adv. Water Resour. 127, 53–75. https://doi.org/10.1016/j.advwatres.2019.03.005.
Hari, V., Rakovec, O., Markonis, Y., Hanel, M., Kumar, R., 2020. Increased future occurrences of the exceptional 2018–2019 central European drought under global warming. Sci. Rep. 10 (1), 12207. https://doi.org/10.1038/s41598-020-68872-9.
Harsányi, E., Bashir, B., Alsilibe, F., Alsafadi, K., Alsalman, A., Széles, A., Rahman, M.H. u., Bácskai, I., Juhász, C., Ratonyi, T., Mohammed, S., 2021. Impact of agricultural drought on sunflower production across Hungary. Atmosphere 12 (10), 1339.
Hauduc, H., Neumann, M.B., Muschalla, D., Gamerith, V., Gillot, S., Vanrolleghem, P.A., 2015. Efficiency criteria for environmental model quality assessment: a review and its application to wastewater treatment. Environ. Model. Softw. 68, 196–204.
He, Q., Wang, M., Liu, K., Li, B., Jiang, Z., 2023. Spatiotemporal analysis of meteorological drought across China based on the high-spatial-resolution multiscale SPI generated by machine learning. Weather Clim. Extremes 40, 100567. https://doi.org/10.1016/j.wace.2023.100567.
Hernández-Morcillo, M., Burgess, P., Mirck, J., Pantera, A., Plieninger, T., 2018. Scanning agroforestry-based solutions for climate change mitigation and adaptation in Europe. Environ. Sci. Policy 80, 44–52. https://doi.org/10.1016/j.envsci.2017.11.013.
Hersi, N.A.M., Mulungu, D.M.M., Nobert, J., 2023. Prediction of future climate in semi-arid catchment under CMIP6 scenarios: A case study of Bahi (Manyoni) catchment in Internal Drainage basin (IDB), Tanzania. Phys. Chem. Earth, Parts a/b/c 129, 103309. https://doi.org/10.1016/j.pce.2022.103309.
Holtanova, E., Belda, M., Halenka, T., 2023. Evaluation of CMIP6 GCMs: the perspective of RCM boundary conditions. In: EGU General Assembly Copernicus Meetings, Vienna, Austria. https://doi.org/10.5194/egusphere-egu23-11741.
Huang, J., Ling, S., Wu, X., Deng, R., 2022. GIS-based comparative study of the Bayesian network, decision table, radial basis function network and stochastic gradient descent for the spatial prediction of landslide susceptibility. Land 11 (3), 436.
Ionita, M., Nagavciuc, V., 2020. Forecasting low flow conditions months in advance through teleconnection patterns, with a special focus on summer 2018. Sci. Rep. 10 (1), 1–12. https://doi.org/10.1038/s41598-020-70060-8.
Ionita, M., Nagavciuc, V., 2021. Changes in drought features at the European level over the last 120 years. Nat. Hazards Earth Syst. Sci. 21 (5), 1685–1701. https://doi.org/10.5194/nhess-21-1685-2021.
Ionita, M., Tallaksen, L.M., Kingston, D.G., Stagge, J.H., Laaha, G., Van Lanen, H.A.J., Scholz, P., Chelcea, S.M., Haslinger, K., 2017. The European 2015 drought from a climatological perspective. Hydrol. Earth Syst. Sci. 21 (3), 1397–1419.
Ionita, M., Nagavciuc, V., Kumar, R., Rakovec, O., 2020. On the curious case of the recent decade, mid-spring precipitation deficit in Central Europe. npj Clim. Atmosp. Sci. 3 (1), 49. https://doi.org/10.1038/s41612-020-00153-8.
Iranshahi, M., Ebrahimi, B., Yousefi, H., Moridi, A., 2023. Investigating the effects of climate change on temperature and precipitation using neural network and CMIP6 (Case study: Aleshtar and Khorramabad Stations). Water Irrigat. Manage. 12 (4), 821–845. https://doi.org/10.22059/jwim.2022.346796.1009.
Jeong, D.I., Sushama, L., Naveed Khaliq, M., 2014. The role of temperature in drought projections over North America. Clim. Change 127 (2), 289–303. https://doi.org/10.1007/s10584-014-1248-3.
Kawai, H., Yukimoto, S., Koshiro, T., Oshima, N., Tanaka, T., Yoshimura, H., Nagasawa, R., 2019. Significant improvement of cloud representation in the global climate model MRI-ESM2. Geosci. Model Dev. 12 (7), 2875–2897.
Khan, N., Sachindra, D.A., Shahid, S., Ahmed, K., Shiru, M.S., Nawaz, N., 2020. Prediction of droughts over Pakistan using machine learning algorithms. Adv. Water Resour. 139, 103562. https://doi.org/10.1016/j.advwatres.2020.103562.
Khanmohammadi, N., Rezaie, H., Behmanesh, J., 2022. Investigation of drought trend on the basis of the best obtained drought index. Water Resour. Manag. 36 (4), 1355–1375. https://doi.org/10.1007/s11269-022-03086-4.
Kohavi, R., 1995. The power of decision tables. In: Lavrac, N., Wrobel, S. (Eds.), Machine Learning: ECML-95. Springer Berlin Heidelberg, Berlin, Heidelberg, pp. 174–189.
Kuswanto, H., Naufal, A., 2019. Evaluation of performance of drought prediction in Indonesia based on TRMM and MERRA-2 using machine learning methods. MethodsX 6, 1238–1251. https://doi.org/10.1016/j.mex.2019.05.029.
Leo, S., De Antoni Migliorati, M., Grace, P.R., 2021. Predicting within-field cotton yields using publicly available datasets and machine learning. Agron. J. 113 (2), 1150–1163. https://doi.org/10.1002/agj2.20543.
Lhotka, O., Kyselý, J., Plavcová, E., 2018. Evaluation of major heat waves' mechanisms in EURO-CORDEX RCMs over Central Europe. Clim. Dyn. 50 (11), 4249–4262. https://doi.org/10.1007/s00382-017-3873-9.
Li, J., Zhou, S., Hu, R., 2016. Hydrological drought class transition using SPI and SRI time series by loglinear regression. Water Resour. Manag. 30 (2), 669–684. https://doi.org/10.1007/s11269-015-1184-7.
Li, J., Wang, Z., Wu, X., Xu, C.-Y., Guo, S., Chen, X., 2020. Toward monitoring short-term droughts using a novel daily scale, standardized antecedent precipitation evapotranspiration index. J. Hydrometeorol. 21 (5), 891–908.
Li, J., Wang, Z., Wu, X., Xu, C.-Y., Guo, S., Chen, X., Zhang, Z., 2021. Robust meteorological drought prediction using antecedent SST fluctuations and machine learning. Water Resour. Res. 57 (8) https://doi.org/10.1029/2020WR029413.
Liaw, A., Wiener, M., 2002. Classification and regression by randomForest. R News 2 (3), 18–22.
Lin, J., Lu, S., He, X., Wang, F., 2021. Analyzing the impact of three-dimensional building structure on CO2 emissions based on random forest regression. Energy 236, 121502. https://doi.org/10.1016/j.energy.2021.121502.
Liu, Z.N., Li, Q.F., Nguyen, L.B., Xu, G.H., 2018. Comparing machine-learning models for drought forecasting in Vietnam's Cai River basin. Pol. J. Environ. Stud. 27 (6), 2633–2646. https://doi.org/10.15244/pjoes/80866.
Lotfirad, M., Esmaeili-Gisavandani, H., Adib, A., 2021. Drought monitoring and prediction using SPI, SPEI, and random forest model in various climates of Iran. J. Water Clim. Change 13 (2), 383–406. https://doi.org/10.2166/wcc.2021.287.
Lotfirad, M., Esmaeili-Gisavandani, H., Adib, A., 2022. Drought monitoring and prediction using SPI, SPEI, and random forest model in various climates of Iran. J. Water Clim. Change 13 (2), 383–406. https://doi.org/10.2166/wcc.2021.287.
Luterbacher, J., Dietrich, D., Xoplaki, E., Grosjean, M., Wanner, H., 2004. European seasonal and annual temperature variability, trends, and extremes since 1500. Science 303 (5663), 1499–1503. https://doi.org/10.1126/science.1093877.
Maca, P., Pech, P., 2016. Forecasting SPEI and SPI drought indices using the integrated artificial neural networks. Comput. Intell. Neurosci. 2016, 3868519 https://doi.org/10.1155/2016/3868519.
Magnan, A.K., Pörtner, H.-O., Duvat, V.K.E., Garschagen, M., Guinder, V.A., Zommers, Z., Hoegh-Guldberg, O., Gattuso, J.-P., 2021. Estimating the global risk of anthropogenic climate change. Nat. Clim. Chang. 11 (10), 879–885.
McKee, T.B., Doesken, N.J., Kleist, J., 1993. The relationship of drought frequency and duration to time scales. In: Proceedings of the 8th Conference on Applied Climatology. California, pp. 179–183.
Mohammed, S., Elbeltagi, A., Bashir, B., Alsafadi, K., Alsilibe, F., Alsalman, A., Zeraatpisheh, M., Széles, A., Harsányi, E., 2022. A comparative analysis of data mining techniques for agricultural and hydrological drought prediction in the eastern Mediterranean. Comput. Electron. Agric. 197, 106925. https://doi.org/10.1016/j.compag.2022.106925.
Mondal, S.K., Tao, H., Huang, J., Wang, Y., Su, B., Zhai, J., Jing, C., Wen, S., Jiang, S., Chen, Z., Jiang, T., 2021. Projected changes in temperature, precipitation and potential evapotranspiration across Indus River Basin at 1.5–3.0 °C warming levels using CMIP6-GCMs. Sci. Total Environ. 789, 147867. https://doi.org/10.1016/j.scitotenv.2021.147867.
Montesinos López, O.A., Montesinos López, A., Crossa, J., 2022. Overfitting, model tuning, and evaluation of prediction performance. In: Montesinos López, O.A., Montesinos López, A., Crossa, J. (Eds.), Multivariate Statistical Machine Learning Methods for Genomic Prediction. Springer International Publishing, Cham, pp. 109–139.

Nafii, A., Taleb, A., El Mesbahi, M., Ezzaouini, M.A., El Bilali, A., 2023. Early forecasting hydrological and agricultural droughts in the Bouregreg Basin using a machine learning approach. Water 15 (1), 122.
Nash, J.E., Sutcliffe, J.V., 1970. River flow forecasting through conceptual models part I — A discussion of principles. J. Hydrol. 10 (3), 282–290. https://doi.org/10.1016/0022-1694(70)90255-6.
Nikulin, G., Kjellström, E., Hansson, U., Strandberg, G., Ullerstig, A., 2011. Evaluation and future projections of temperature, precipitation and wind extremes over Europe in an ensemble of regional climate simulations. Tellus A 63 (1), 41–55. https://doi.org/10.1111/j.1600-0870.2010.00466.x.
Oikonomou, P.D., Karavitis, C.A., Tsesmelis, D.E., Kolokytha, E., Maia, R., 2020. Drought characteristics assessment in Europe over the past 50 years. Water Resour. Manag. 34 (15), 4757–4772. https://doi.org/10.1007/s11269-020-02688-0.
O'Neill, B.C., Tebaldi, C., van Vuuren, D.P., Eyring, V., Friedlingstein, P., Hurtt, G., Knutti, R., Kriegler, E., Lamarque, J.-F., Lowe, J., Meehl, G.A., Moss, R., Riahi, K., Sanderson, B.M., 2016. The scenario model intercomparison project (ScenarioMIP) for CMIP6. Geosci. Model Dev. 9 (9), 3461–3482.
Othman, W.Z., Tukimat, N.N.A., 2023. Assessment on the climate change impact using CMIP6. IOP Conf. Ser.: Earth Environ. Sci. 1140 (1), 012005 https://doi.org/10.1088/1755-1315/1140/1/012005.
Palmer, T.E., Booth, B.B.B., McSweeney, C.F., 2021. How does the CMIP6 ensemble change the picture for European climate projections? Environ. Res. Lett. 16 (9), 094042 https://doi.org/10.1088/1748-9326/ac1ed9.
Pande, C.B., Costache, R., Sammen, S.S., Noor, R., Elbeltagi, A., 2023. Combination of data-driven models and best subset regression for predicting the standardized precipitation index (SPI) at the upper Godavari Basin in India. Theor. Appl. Climatol. 152 (1), 535–558. https://doi.org/10.1007/s00704-023-04426-z.
Park, S., Im, J., Jang, E., Rhee, J., 2016. Drought assessment and monitoring through blending of multi-sensor indices using machine learning approaches for different climate regions. Agric. For. Meteorol. 216, 157–169. https://doi.org/10.1016/j.agrformet.2015.10.011.
Park, S., Seo, E., Kang, D., Im, J., Lee, M.-I., 2018. Prediction of drought on pentad scale using remote sensing data and MJO index through random Forest over East Asia. Remote Sens. (Basel) 10 (11), 1811. https://doi.org/10.3390/rs10111811.
Pearson, K., Henrici, O.M.F.E., 1896. VII. Mathematical contributions to the theory of evolution.—III. Regression, heredity, and panmixia. Philos. Trans. R. Soc. Lond. Ser. A, Contain. Pap. Math. Phys. Charact. 187, 253–318. https://doi.org/10.1098/rsta.1896.0007.
Pham, B.T., Vu, V.D., Costache, R., Phong, T.V., Ngo, T.Q., Tran, T.-H., Nguyen, H.D., Amiri, M., Tan, M.T., Trinh, P.T., Le, H.V., Prakash, I., 2022. Landslide susceptibility mapping using state-of-the-art machine learning ensembles. Geocarto Int. 37 (18), 5175–5200.
Pimonsree, S., Kamworapan, S., Gheewala, S.H., Thongbhakdi, A., Prueksakorn, K., 2023. Evaluation of CMIP6 GCMs performance to simulate precipitation over Southeast Asia. Atmos. Res. 282, 106522 https://doi.org/10.1016/j.atmosres.2022.106522.
Plavcová, E., Beranová, R., Huth, R., Lhotka, O., 2023. Projected changes in precipitation variability over Europe in CMIP6 climate models. Copernicus Meetings.
Pörtner, H.-O. et al., 2022. Climate change 2022: Impacts, adaptation and vulnerability. IPCC Sixth Assessment Report.
Poschlod, B., 2022. Attributing heavy rainfall event in Berchtesgadener land to recent climate change – Further rainfall intensification projected for the future. Weather Clim. Extremes 38, 100492. https://doi.org/10.1016/j.wace.2022.100492.
Pourghasemi, H.R., Kariminejad, N., Amiri, M., Edalat, M., Zarafshar, M., Blaschke, T., Cerda, A., 2020. Assessing and mapping multi-hazard risk susceptibility using a machine learning technique. Sci. Rep. 10 (1) https://doi.org/10.1038/s41598-020-60191-3.
Prodhan, F.A., Zhang, J., Hasan, S.S., Pangali Sharma, T.P., Mohana, H.P., 2022. A review of machine learning methods for drought hazard monitoring and forecasting: Current research trends, challenges, and future research directions. Environ. Model. Softw. 149, 105327. https://doi.org/10.1016/j.envsoft.2022.105327.
Qiu, J., Shen, Z., Xie, H., 2023. Drought impacts on hydrology and water quality under climate change. Sci. Total Environ. 858, 159854 https://doi.org/10.1016/j.scitotenv.2022.159854.
Quinlan, J.R., 1992. Learning with continuous classes, 5th Australian joint conference on artificial intelligence. World Scientific 343–348.
Rahmati, O., Falah, F., Dayal, K.S., Deo, R.C., Mohammadi, F., Biggs, T., Moghaddam, D. D., Naghibi, S.A., Bui, D.T., 2020. Machine learning approaches for spatial modeling of agricultural droughts in the south-east region of Queensland Australia. Sci. Total Environ. 699, 134230. https://doi.org/10.1016/j.scitotenv.2019.134230.
Rajczak, J., Schär, C., 2017. Projections of future precipitation extremes over Europe: A multimodel assessment of climate simulations. J. Geophys. Res. Atmos. 122 (20), 10773–10800. https://doi.org/10.1002/2017JD027176.
Rhee, J., Im, J., 2017. Meteorological drought forecasting for ungauged areas based on machine learning: Using long-range climate forecast and remote sensing data. Agric. For. Meteorol. 237–238, 105–122. https://doi.org/10.1016/j.agrformet.2017.02.011.
Saha, S., Gogoi, P., Gayen, A., Paul, G.C., 2021. Constructing the machine learning techniques based spatial drought vulnerability index in Karnataka state of India. J. Clean. Prod. 314, 128073 https://doi.org/10.1016/j.jclepro.2021.128073.
Saha, U., Sateesh, M., 2022. Rainfall extremes on the rise: observations during 1951–2020 and bias-corrected CMIP6 projections for near- and late 21st century over Indian landmass. J. Hydrol. 608, 127682 https://doi.org/10.1016/j.jhydrol.2022.127682.
Samantaray, A.K., Ramadas, M., Panda, R.K., 2022. Changes in drought characteristics based on rainfall pattern drought index and the CMIP6 multi-model ensemble. Agric. Water Manag. 266, 107568 https://doi.org/10.1016/j.agwat.2022.107568.
Sauter, C., Fowler, H.J., Westra, S., Ali, H., Peleg, N., White, C.J., 2023. Compound extreme hourly rainfall preconditioned by heatwaves most likely in the mid-latitudes. Weather Clim. Extremes 40, 100563. https://doi.org/10.1016/j.wace.2023.100563.
Schär, C., Vidale, P.L., Lüthi, D., Frei, C., Häberli, C., Liniger, M.A., Appenzeller, C., 2004. The role of increasing temperature variability in European summer heatwaves. Nature 427 (6972), 332–336. https://doi.org/10.1038/nature02300.
Schuldt, B., Buras, A., Arend, M., Vitasse, Y., Beierkuhnlein, C., Damm, A., Gharun, M., Grams, T.E.E., Hauck, M., Hajek, P., Hartmann, H., Hiltbrunner, E., Hoch, G., Holloway-Phillips, M., Körner, C., Larysch, E., Lübbe, T., Nelson, D.B., Rammig, A., Rigling, A., Rose, L., Ruehr, N.K., Schumann, K., Weiser, F., Werner, C., Wohlgemuth, T., Zang, C.S., Kahmen, A., 2020. A first assessment of the impact of the extreme 2018 summer drought on central European forests. Basic Appl. Ecol. 45, 86–103. https://doi.org/10.1016/j.baae.2020.04.003.
Scranton, P., 2022. Introduction: Hungary—Geography, History, and Society to 1945. In: Scranton, P. (Ed.), Business Practice in Socialist Hungary, Volume 1: Creating the Theft Economy, 1945–1957. Springer International Publishing, Cham, pp. 1–18. https://doi.org/10.1007/978-3-030-89184-8_1.
Sen, P.K., 1968. Estimates of the regression coefficient based on Kendall's Tau. J. Am. Stat. Assoc. 63 (324), 1379–1389. https://doi.org/10.1080/01621459.1968.10480934.
Sihag, P., Mohsenzadeh Karimi, S., Angelaki, A., 2019. Random forest, M5P and regression analysis to estimate the field unsaturated hydraulic conductivity. Appl. Water Sci. 9 (5), 129. https://doi.org/10.1007/s13201-019-1007-8.
Spinoni, J., Barbosa, P., De Jager, A., McCormick, N., Naumann, G., Vogt, J.V., Magni, D., Masante, D., Mazzeschi, M., 2019. A new global database of meteorological drought events from 1951 to 2016. J. Hydrol.: Reg. Stud. 22, 100593. https://doi.org/10.1016/j.ejrh.2019.100593.
Su, B., Huang, J., Mondal, S.K., Zhai, J., Wang, Y., Wen, S., Gao, M., Lv, Y., Jiang, S., Jiang, T., Li, A., 2021. Insight from CMIP6 SSP-RCP scenarios for future drought characteristics in China. Atmos. Res. 250, 105375. https://doi.org/10.1016/j.atmosres.2020.105375.
Swart, N.C., Cole, J.N.S., Kharin, V.V., Lazare, M., Scinocca, J.F., Gillett, N.P., Anstey, J., Arora, V., Christian, J.R., Hanna, S., Jiao, Y., Lee, W.G., Majaess, F., Saenko, O.A., Seiler, C., Seinen, C., Shao, A., Sigmond, M., Solheim, L., von Salzen, K., Yang, D., Winter, B., 2019. The Canadian Earth System Model version 5 (CanESM5.0.3). Geosci. Model Dev. 12 (11), 4823–4873.
Tatebe, H., Ogura, T., Nitta, T., Komuro, Y., Ogochi, K., Takemura, T., Sudo, K., Sekiguchi, M., Abe, M., Saito, F., Chikira, M., Watanabe, S., Mori, M., Hirota, N., Kawatani, Y., Mochizuki, T., Yoshimura, K., Takata, K., O'ishi, R., Yamazaki, D., Suzuki, T., Kurogi, M., Kataoka, T., Watanabe, M., Kimoto, M., 2019. Description and basic evaluation of simulated mean state, internal variability, and climate sensitivity in MIROC6. Geosci. Model Dev. 12 (7), 2727–2765.
Taylor, K.E., 2001. Summarizing multiple aspects of model performance in a single diagram. J. Geophys. Res. Atmos. 106 (D7), 7183–7192. https://doi.org/10.1029/2000JD900719.
Theil, H., 1950. A rank-invariant method of linear and polynominal regression analysis (Parts 1–3). Ned. Akad. Wetensch. Proc. Ser. A 1397–1412.
Tomczyk, A.M., Bednorz, E., 2019. Heat waves in Central Europe and tropospheric anomalies of temperature and geopotential heights. Int. J. Climatol. 39 (11), 4189–4205. https://doi.org/10.1002/joc.6067.
Ullah, I., Ma, X., Asfaw, T.G., Yin, J., Iyakaremye, V., Saleem, F., Xing, Y., Azam, K., Syed, S., 2022. Projected changes in increased drought risks over South Asia under a warmer climate. Earth's Future 10 (10). https://doi.org/10.1029/2022EF002830.
Vadas, A., 2022. Geography, Natural Resources, and Environment. Oxford Handbook of Medieval Central Europe: 23.
Van Lanen, H.A.J., Laaha, G., Kingston, D.G., Gauster, T., Ionita, M., Vidal, J.-P., Vlnas, R., Tallaksen, L.M., Stahl, K., Hannaford, J., Delus, C., Fendekova, M., Mediero, L., Prudhomme, C., Rets, E., Romanowicz, R.J., Gailliez, S., Wong, W.K., Adler, M.-J., Blauhut, V., Caillouet, L., Chelcea, S., Frolova, N., Gudmundsson, L., Hanel, M., Haslinger, K., Kireeva, M., Osuch, M., Sauquet, E., Stagge, J.H., Van Loon, A.F., 2016. Hydrology needed to manage droughts: the 2015 European case. Hydrol. Process. 30 (17), 3097–3104.
Wahla, S.S., Kazmi, J.H., Sharifi, A., Shirazi, S.A., Tariq, A., Joyell Smith, H., 2024. Assessing spatio-temporal mapping and monitoring of climatic variability using SPEI and RF machine learning models. Geocarto Int. 37 (27), 14963–14982. https://doi.org/10.1080/10106049.2022.2093411.
Wang, T., Tu, X., Singh, V.P., Chen, X., Lin, K., 2021. Global data assessment and analysis of drought characteristics based on CMIP6. J. Hydrol. 596, 126091 https://doi.org/10.1016/j.jhydrol.2021.126091.
Willmott, C.J., Ackleson, S.G., Davis, R.E., Feddema, J.J., Klink, K.M., Legates, D.R., O'Donnell, J., Rowe, C.M., 1985. Statistics for the evaluation and comparison of models. J. Geophys. Res. Oceans 90 (C5), 8995–9005.
Wu, C., J.-F. Yeh, P., Chen, Y.-Y., Lv, W., Hu, B.X., Huang, G., 2021. Copula-based risk evaluation of global meteorological drought in the 21st century based on CMIP5 multi-model ensemble projections. J. Hydrol. 598, 126265. https://doi.org/10.1016/j.jhydrol.2021.126265.
Xu, Z.X., Takeuchi, K., Ishidaira, H., 2003. Monotonic trend and step changes in Japanese precipitation. J. Hydrol. 279 (1), 144–150. https://doi.org/10.1016/S0022-1694(03)00178-1.
Xu, P., Wang, D., Wang, Y., Singh, V.P., Qiu, J., Wu, J., Zhang, A., Ju, X., 2023. + Dynamic identification and risk analysis of compound dry-hot events considering

nonstationarity. J. Hydrol. 616, 128852. https://doi.org/10.1016/j.jhydrol.2022.128852.
Yang, J., Chang, J., Wang, Y., Li, Y., Hu, H., Chen, Y., Huang, Q., Yao, J., 2018. Comprehensive drought characteristics analysis based on a nonlinear multivariate drought index. J. Hydrol. 557, 651–667.
Yaseen, Z.M., Ali, M., Sharafati, A., Al-Ansari, N., Shahid, S., 2021. Forecasting standardized precipitation index using data intelligence models: regional investigation of Bangladesh. Sci. Rep. 11 (1), 3435. https://doi.org/10.1038/s41598-021-82977-9.
Yerdelen, C., Abdelkader, M., Eris, E., 2021. Assessment of drought in SPI series using continuous wavelet analysis for Gediz Basin, Turkey. Atmos. Res. 260, 105687 https://doi.org/10.1016/j.atmosres.2021.105687.
Yuce, M.I., Esit, M., Kalaycioglu, V., 2023. Investigation of trends in extreme events: a case study of Ceyhan Basin, Turkey. J. Appl. Water Eng. Res. 11 (3), 317–332.
Zeybekoğlu, U., Aktürk, G., 2021. A comparison of the China-Z Index (CZI) and the Standardized Precipitation Index (SPI) for drought assessment in the Hirfanli Dam basin in Central Turkey. Arab. J. Geosci. 14 (24), 2731. https://doi.org/10.1007/s12517-021-09095-8.
Zhang, R., Chen, Z.-Y., Xu, L.-J., Ou, C.-Q., 2019. Meteorological drought forecasting based on a statistical model with machine learning techniques in Shaanxi province, China. Sci. Total Environ. 665, 338–346. https://doi.org/10.1016/j.scitotenv.2019.01.431.
Zhang, X., Hua, L., Jiang, D., 2022. Assessment of CMIP6 model performance for temperature and precipitation in Xinjiang, China. Atmos. Ocean. Sci. Lett. 15 (2), 100128 https://doi.org/10.1016/j.aosl.2021.100128.
Zhang, R., Sun, C., Zhu, J., Zhang, R., Li, W., 2020. Increased European heat waves in recent decades in response to shrinking Arctic Sea ice and Eurasian snow cover. npj Clim. Atmos. Sci. 3 (1), 7. https://doi.org/10.1038/s41612-020-0110-8.
Zhao, C., Brissette, F., Chen, J., 2023. Projection of future extreme meteorological droughts using two large multi-member climate model ensembles. J. Hydrol. 618, 129155 https://doi.org/10.1016/j.jhydrol.2023.129155.
Zounemat-Kermani, M., Batelaan, O., Fadaee, M., Hinkelmann, R., 2021. Ensemble machine learning paradigms in hydrology: A review. J. Hydrol. 598, 126266 https://doi.org/10.1016/j.jhydrol.2021.126266.